Mathematical Models and Methods in Applied Sciences
Vol. 30, No. 3 (2020) 477–512

DOI: 10.1142/S0218202520500128

World Scientific
www.worldscientific.com

The Stokes complex for Virtual Elements in three dimensions

L. Beirão da Veiga*, F. Dassi† and G. Vacca‡
Dipartimento di Matematica e Applicazioni, Università di Milano Bicocca,
Via Roberto Cozzi 55, 20126 Milano, Italy
**lourenco.beirao@unimib.it*
†*franco.dassi@unimib.it*
‡*giuseppe.vacca@unimib.it*

Received 29 January 2019
Revised 12 November 2019
Accepted 14 November 2019
Published 23 March 2020
Communicated by F. Brezzi

This paper has two objectives. On one side, we develop and test numerically divergence-free Virtual Elements in three dimensions, for variable "polynomial" order. These are the natural extension of the two-dimensional divergence-free VEM elements, with some modification that allows for a better computational efficiency. We test the element's performance both for the Stokes and (diffusion dominated) Navier–Stokes equation. The second, and perhaps main, motivation is to show that our scheme, also in three dimensions, enjoys an underlying discrete Stokes complex structure. We build a pair of virtual discrete spaces based on general polytopal partitions, the first one being scalar and the second one being vector valued, such that when coupled with our velocity and pressure spaces, yield a discrete Stokes complex.

Keywords: Virtual elements; Stokes complex; Navier–Stokes equation; polygonal meshes.

AMS Subject Classification: 65N30, 76D05

1. Introduction

The Virtual Element Method (VEM) was introduced in Refs. 10 and 12 as a generalization of the Finite Element Method (FEM) allowing for general polytopal meshes. Nowadays the VEM technology has reached a good level of success; among the many papers we here limit ourselves in citing a few sample works.[3,6,11,21,22,34,41,51] It was soon recognized that the flexibility of VEM allows to build elements that hold peculiar advantages also on more standard grids. One main example is that of "divergence-free" Virtual Elements for Stokes-type problems, initiated in Refs. 5 and 17 and further developed in Refs. 18 and 57. An advantage of

‡Corresponding author.

the proposed family of Virtual Elements is that, without the need of a high minimal polynomial degree as it happens in conforming FEM, it is able to yield a discrete divergence-free (conforming) velocity solution, which can be an interesting asset as explored for Finite Elements in Refs. 44, 45, 46, 48 and 53. For a wider look in the literature, other VEM for Stokes-type problems can be found in Refs. 28, 29, 31, 35, 42 and 50 while different polygonal methods for the same problem in Refs. 24, 33, 38 and 49.

This paper has two objectives. On one side, we develop and test numerically for the first time the divergence-free Virtual Elements in three dimensions (for variable "polynomial" order k). These are the natural extension of the two-dimensional (2D) VEM elements of Refs. 17 and 18, with some modification that allows for a better computational efficiency. We first test the element's performance for the Stokes and (diffusion dominated) Navier–Stokes equation for different kind of meshes (such as Voronoi, but also cubes and tetrahedra) and then show a specific test that underlines the divergence-free property (in the spirit of Refs. 18 and 48).

The second, and perhaps main, motivation is to show that our scheme, also in three dimensions, enjoys an underlying discrete Stokes complex structure. That is, a discrete structure of the kind

$$\mathbb{R} \xrightarrow{\ i\ } W_h \xrightarrow{\ \nabla\ } \boldsymbol{\Sigma}_h \xrightarrow{\ \mathbf{curl}\ } \boldsymbol{V}_h \xrightarrow{\ \mathrm{div}\ } Q_h \xrightarrow{\ 0\ } 0,$$

where the image of each operator exactly corresponds to the kernel of the following one, thus mimicking the continuous complex

$$\mathbb{R} \xrightarrow{\ i\ } H^1(\Omega) \xrightarrow{\ \nabla\ } \boldsymbol{\Sigma}(\Omega) \xrightarrow{\ \mathbf{curl}\ } [H^1(\Omega)]^3 \xrightarrow{\ \mathrm{div}\ } L^2(\Omega) \xrightarrow{\ 0\ } 0,$$

with $\boldsymbol{\Sigma}(\Omega)$ denoting functions of $L^2(\Omega)$ with $\mathbf{curl}$ in $H^1(\Omega)$.[4,43] Discrete Stokes complexes have been extensively studied in the literature of Finite Elements since the presence of an underlying complex implies a series of interesting advantages (such as the divergence-free property), in addition to guaranteeing that the discrete scheme is able to correctly mimic the structure of the problem under study.[7–9,27,36,37,39,40,52] This motivation is therefore mainly theoretical in nature, but it serves the important purpose of giving a deeper foundation to our method. We therefore build a pair of virtual discrete spaces based on general polytopal partitions of Ω, the first one W_h, conforming in $H^1(\Omega)$ and the second one $\boldsymbol{\Sigma}_h$ conforming in $\boldsymbol{\Sigma}(\Omega)$, such that, when coupled with our velocity and pressure spaces, yield a discrete Stokes complex. We also build a set of carefully chosen associated degrees of freedom (DoFs). This construction was already developed in two dimensions in Ref. 19, but here things are more involved due to the much more complex nature of the curl operator in 3D when compared to 2D. In this respect we must underline that, to the best of the authors knowledge, no Stokes exact complex of the type above exists for conforming Finite Elements in three dimensions. There exist FEM for different (more regular) Stokes complexes, but at the price of developing cumbersome elements with a large minimal polynomial degree (we refer to Ref. 46 for an overview)

or using a subdivision of the element.[32] We finally note that our construction holds for a general "polynomial" order $k \geq 2$.

The paper is organized as follows. After introducing some notation and preliminaries in Sec. 2, the Virtual Element spaces and the associated DoFs are deployed in Sec. 3. In Sec. 4, we prove that the introduced spaces constitute an exact complex. In Sec. 5, we describe the discrete problem, together with the associated projectors and bilinear forms. In Sec. 6, we provide the numerical tests. Finally, in the appendix we prove a useful lemma.

2. Notations and Preliminaries

In this section, we introduce some basic tools and notations useful in the construction and theoretical analysis of VEMs.

Throughout the paper, we will follow the usual notation for Sobolev spaces and norms.[1] Hence, for an open bounded domain ω, the norms in the spaces $W_p^s(\omega)$ and $L^p(\omega)$ are denoted by $\|\cdot\|_{W_p^s(\omega)}$ and $\|\cdot\|_{L^p(\omega)}$, respectively. Norm and seminorm in $H^s(\omega)$ are denoted respectively by $\|\cdot\|_{s,\omega}$ and $|\cdot|_{s,\omega}$, while $(\cdot,\cdot)_\omega$ and $\|\cdot\|_\omega$ denote the L^2-inner product and the L^2-norm (the subscript ω may be omitted when ω is the whole computational domain Ω).

2.1. *Basic notations and mesh assumptions*

From now on, we will denote with P a general polyhedron having ℓ_V vertexes V, ℓ_e edges e and ℓ_f faces f.

For each polyhedron P, each face f of P and each edge e of f we denote with:

- $\boldsymbol{n}_P^f$ (respectively, $\boldsymbol{n}_P$) the unit outward normal vector to f (respectively, to ∂P),
- $\boldsymbol{n}_f^e$ (respectively, $\boldsymbol{n}_f$) the unit vector in the plane of f that is normal to the edge e (respectively, to ∂f) and outward with respect to f,
- $\boldsymbol{t}_f^e$ (respectively, $\boldsymbol{t}_f$) the unit vector tangent to e (respectively, to ∂f) counterclockwise with respect to $\boldsymbol{n}_P^f$,
- $\boldsymbol{\tau}_1^f$ and $\boldsymbol{\tau}_2^f$ two orthogonal unit vectors lying on f and such that $\boldsymbol{\tau}_1^f \wedge \boldsymbol{\tau}_2^f = \boldsymbol{n}_P^f$, i.e. $\boldsymbol{\tau}_f^1$ and $\boldsymbol{\tau}_f^2$ constitute the axis of a local coordinate system on f (see also Sec. 2.2),
- $\boldsymbol{t}_e$ a unit vector tangent to the edge e.

Notice that the vectors $\boldsymbol{t}_f^e$, $\boldsymbol{t}_f$, $\boldsymbol{\tau}_1^f$ and $\boldsymbol{\tau}_2^f$ actually depend on P (we do not write such dependence explicitly for lightening the notations).

In the following $\mathcal{O}$ will denote a general geometrical entity (element, face, edge) having diameter $h_\mathcal{O}$.

Let Ω be the computational domain that we assume to be a contractible polyhedron (i.e. simply connected polyhedron with boundary $\partial\Omega$ which consists of one connected component), with Lipschitz boundary. Let $\{\Omega_h\}_h$ be a sequence of decompositions of Ω into general polyhedral elements P where $h := \sup_{P\in\Omega_h} h_P$.

We suppose that for all h, each element P in Ω_h is a contractible polyhedron that fulfills the following assumptions:

(A1) P is star-shaped with respect to a ball B_P of radius $\geq \varrho h_P$,
(A2) every face f of P is star-shaped with respect to a disk B_f of radius $\geq \varrho h_P$,
(A3) every edge e in P satisfies $h_e \geq \varrho h_P$,

where ϱ is a uniform positive constant. We remark that the hypotheses **(A1)**–**(A3)**, though not too restrictive in many practical cases, can be further relaxed, as investigated in Refs. 16, 25, 26 and 30.

The total number of vertexes, edges, faces and elements in the decomposition Ω_h are denoted respectively with L_V, L_e, L_f, L_P.

For any mesh object $\mathcal{O}$ and for $n \in \mathbb{N}$ we introduce the spaces:

- $\mathbb{P}_n(\mathcal{O})$ the polynomials on $\mathcal{O}$ of degree $\leq n$ (with the extended notation $\mathbb{P}_{-1}(\mathcal{O}) = \{0\}$),
- $\widehat{\mathbb{P}}_{n\setminus m}(\mathcal{O}) := \mathbb{P}_n(\mathcal{O})\setminus\mathbb{P}_m(\mathcal{O})$ for $m < n$, denotes the polynomials in $\mathbb{P}_n(\mathcal{O})$ with monomials of degree strictly greater than m.

Moreover, for any mesh object $\mathcal{O}$ of dimension d we define

$$\pi_{n,d} := \dim(\mathbb{P}_n(\mathcal{O})) = \dim(\mathbb{P}_n(\mathbb{R}^d)), \tag{2.1}$$

and thus $\dim(\widehat{\mathbb{P}}_{n\setminus m}(\mathcal{O})) = \pi_{n,d} - \pi_{m,d}$.

In the following the symbol $\lesssim$ will denote a bound up to a generic positive constant, independent of the mesh size h, but which may depend on Ω, on the "polynomial" order k and on the shape constant ϱ in assumptions **(A1)**–**(A3)**.

2.2. *Vector calculus and de Rham complexes*

Here below we fix some additional notation of the multivariable calculus.

Three-dimensional (3D) operators. In three dimensions we denote with $\boldsymbol{x} = (x_1, x_2, x_3)$ the independent variable. With a usual notation the symbols ∇ and Δ denote the gradient and Laplacian for scalar functions, while $\boldsymbol{\Delta}$, $\boldsymbol{\nabla}$, $\boldsymbol{\varepsilon}$, div and **curl** denote the vector Laplacian, the gradient and the symmetric gradient operator, the divergence and the curl operator for vector fields. Note that on each polyhedron P the following useful polynomial decompositions hold:

$$[\mathbb{P}_n(P)]^3 = \nabla(\mathbb{P}_{n+1}(P)) \oplus (\boldsymbol{x} \wedge [\mathbb{P}_{n-1}(P)]^3), \tag{2.2}$$

$$[\mathbb{P}_n(P)]^3 = \mathbf{curl}(\mathbb{P}_{n+1}(P)) \oplus \boldsymbol{x}\,\mathbb{P}_{n-1}(P). \tag{2.3}$$

Tangential operators. Let f be a face of a polyhedron P, we denote with $\boldsymbol{x}_f := (x_{f_1}, x_{f_2})$ the independent variable (i.e. a local coordinate system on f associated with the axes $\boldsymbol{\tau}_f^1$ and $\boldsymbol{\tau}_f^2$ introduced above). The tangential differential operators are denoted by a subscript f. Therefore, the symbols ∇_f and Δ_f denote the gradient and Laplacian for scalar functions. For instance if f lies on the plane $x_3 = 0$ and $\boldsymbol{\tau}_f^1$

and $\boldsymbol{\tau}_f^2$ are associated with the coordinate system (x_1, x_2) then $\nabla_f\varphi = \left(\frac{\partial\varphi}{\partial x_1}, \frac{\partial\varphi}{\partial x_2}\right)$ and $\Delta_f\varphi = \frac{\partial^2\varphi}{\partial x_1^2} + \frac{\partial^2\varphi}{\partial x_2^2}$, while $\nabla\varphi = \left(\frac{\partial\varphi}{\partial x_1}, \frac{\partial\varphi}{\partial x_2}, \frac{\partial\varphi}{\partial x_3}\right)$ and $\Delta\varphi = \frac{\partial^2\varphi}{\partial x_1^2} + \frac{\partial^2\varphi}{\partial x_2^2} + \frac{\partial^2\varphi}{\partial x_3^2}$. In the same way $\boldsymbol{\Delta}_f$, $\boldsymbol{\nabla}_f$, and div_f denote the vector Laplacian, the gradient operator and the divergence for vector fields on f (with respect to the coordinate $\boldsymbol{x}_f$). Furthermore for a scalar function φ and a vector field $\boldsymbol{v} := (v_1, v_2)$ we set

$$\mathbf{rot}_f\varphi := \left(\frac{\partial\varphi}{\partial x_{f_2}}, -\frac{\partial\varphi}{\partial x_{f_1}}\right) \quad \text{and} \quad \mathrm{rot}_f\boldsymbol{v} := \frac{\partial v_2}{\partial x_{f_1}} - \frac{\partial v_1}{\partial x_{f_2}}.$$

The following two-dimensional polynomial decompositions hold

$$[\mathbb{P}_n(f)]^2 = \nabla_f(\mathbb{P}_{n+1}(f)) \oplus \boldsymbol{x}_f^{\perp}\,\mathbb{P}_{n-1}(f),$$
$$[\mathbb{P}_n(f)]^2 = \mathbf{rot}_f(\mathbb{P}_{n+1}(f)) \oplus \boldsymbol{x}_f\,\mathbb{P}_{n-1}(f),$$

where $\boldsymbol{x}_f^{\perp} := (x_{f_2}, -x_{f_1})$.

Given a 3D vector-valued function $\boldsymbol{v}$ defined in P, the tangential component $\boldsymbol{v}_f$ of $\boldsymbol{v}$ with respect to the face f is defined by

$$\boldsymbol{v}_f := \boldsymbol{v} - (\boldsymbol{v}\cdot\boldsymbol{n}_P^f)\boldsymbol{n}_P^f.$$

Noticing that $\boldsymbol{v}_f$ is a 3D vector field tangent to f, with a slight abuse of notations we define the 2D vector field $\boldsymbol{v}_\tau$ on ∂P, such that on each face f its restriction to the face f satisfies

$$\boldsymbol{v}_\tau(\boldsymbol{x}_f) = \boldsymbol{v}_f(\boldsymbol{x}).$$

The 3D function $\boldsymbol{v}$ and its 2D tangential restriction $\boldsymbol{v}_\tau$ are related by the **curl**-rot compatibility condition

$$\mathbf{curl}\,\boldsymbol{v}\cdot\boldsymbol{n}_P^f = \mathrm{rot}_f\,\boldsymbol{v}_\tau \quad \text{on any } f\in\partial P. \tag{2.4}$$

Moreover, the Gauss theorem ensures the following rot-tangent component relation

$$\int_f \mathrm{rot}_f\,\boldsymbol{v}_\tau\,\mathrm{d}f = \int_{\partial f}\boldsymbol{v}\cdot\boldsymbol{t}_f\,\mathrm{d}s \quad \text{for any } f\in\partial P. \tag{2.5}$$

Finally, for any scalar function v defined in P, we denote with v_τ the scalar function defined in ∂P such that

$$v_\tau(\boldsymbol{x}_f) := v(\boldsymbol{x})_{|f} \quad \text{on each face } f\in\partial P.$$

On a generic mesh object $\mathcal{O}$ with geometrical dimension d, on a face f and on a polyhedron P we define the following functional spaces:

$$L_0^2(\mathcal{O}) := \left\{v\in L^2(\mathcal{O}) \text{ s.t. } \int_{\mathcal{O}} v\,\mathrm{d}\mathcal{O} = 0\right\},$$
$$\boldsymbol{Z}(\mathcal{O}) := \{\boldsymbol{v}\in[H^1(\mathcal{O})]^2 \text{ s.t. } \mathrm{div}\,\boldsymbol{v} = 0 \text{ in } \mathcal{O}\},$$
$$\boldsymbol{H}(\mathrm{div},\mathcal{O}) := \{\boldsymbol{v}\in[L^2(\mathcal{O})]^d \text{ with } \mathrm{div}\,\boldsymbol{v}\in L^2(\mathcal{O})\},$$
$$\boldsymbol{H}(\mathrm{rot},f) := \{\boldsymbol{v}\in[L^2(f)]^2 \text{ with } \mathrm{rot}_f\,\boldsymbol{v}\in L^2(f)\},$$

$$\boldsymbol{H}(\mathbf{curl},\, P) := \{\boldsymbol{v} \in [L^2(P)]^3 \text{ with } \mathbf{curl}\, \boldsymbol{v} \in [L^2(P)]^3\},$$
$$\boldsymbol{\Sigma}(P) := \{\boldsymbol{v} \in [L^2(P)]^3 \text{ with } \mathbf{curl}\, \boldsymbol{v} \in [H^1(P)]^3\},$$
$$\boldsymbol{\Psi}(P) := \{\boldsymbol{v} \in [L^2(P)]^3 \text{ s.t. } \operatorname{div} \boldsymbol{v} \in H^1(P),\ \mathbf{curl}\, \boldsymbol{v} \in [H^1(P)]^3\}$$

with the "homogeneous counterparts"

$$\boldsymbol{Z}_0(\mathcal{O}) := \{\boldsymbol{v} \in \boldsymbol{Z}(\mathcal{O}) \text{ s.t. } \boldsymbol{v} = \mathbf{0} \text{ on } \partial\mathcal{O}\},$$
$$\boldsymbol{H}_0(\operatorname{div}, \mathcal{O}) := \{\boldsymbol{v} \in H(\operatorname{div}, \mathcal{O}) \text{ s.t. } \boldsymbol{v} \cdot \boldsymbol{n}_{\mathcal{O}} = 0 \text{ on } \partial\mathcal{O}\},$$
$$\boldsymbol{H}_0(\operatorname{rot}, f) := \{\boldsymbol{v} \in H(\operatorname{rot}, f) \text{ s.t. } \boldsymbol{v} \cdot \boldsymbol{t}_f = 0 \text{ on } \partial f\},$$
$$\boldsymbol{H}_0(\mathbf{curl}, P) := \{\boldsymbol{v} \in H(\mathbf{curl}, P) \text{ s.t. } \boldsymbol{v}_\tau = \mathbf{0} \text{ on } \partial P\},$$
$$\boldsymbol{\Sigma}_0(P) := \{\boldsymbol{v} \in \boldsymbol{\Sigma}(P) \text{ s.t. } \boldsymbol{v}_\tau = \mathbf{0} \text{ and } \mathbf{curl}\, \boldsymbol{v} = \mathbf{0} \text{ on } \partial P\},$$
$$\boldsymbol{\Psi}_0(P) := \left\{\boldsymbol{v} \in \boldsymbol{\Psi}(P) \text{ s.t. } \int_{\partial P} \boldsymbol{v} \cdot \boldsymbol{n}_P \, \mathrm{d}f = 0,\ \boldsymbol{v}_\tau = \mathbf{0} \text{ and } \mathbf{curl}\, \boldsymbol{v} = \mathbf{0} \text{ on } \partial P\right\}.$$

Remark 2.1. Notice that for each face $f \in \partial P$, the vector fields $\boldsymbol{v}_f$ and $\boldsymbol{v} \wedge \boldsymbol{n}_P^f$ are different. In fact both lie in the plane of the face f, but $\boldsymbol{v}_f$ is $(\pi/2)$-rotation in f (with respect to the axes $\boldsymbol{\tau}_1$ and $\boldsymbol{\tau}_2$) of $\boldsymbol{v} \wedge \boldsymbol{n}_P^f$. For instance let f lie on the plane $x_3 = 0$ with $\boldsymbol{n}_P^f = (0, 0, 1)$, then for a vector field $\boldsymbol{v} = (v_1, v_2, v_3)$ it holds that $\boldsymbol{v}_f = (v_1, v_2, 0)$ and $\boldsymbol{v} \wedge \boldsymbol{n}_P^f = (v_2, -v_1, 0)$. Therefore, both $\boldsymbol{v}_f$ and $\boldsymbol{v} \wedge \boldsymbol{n}_P^f$ lie in the plane of f and $\boldsymbol{v}_f$ is $(\pi/2)$-rotation of $\boldsymbol{v} \wedge \boldsymbol{n}_P^f$ (with respect to the orientation given by $\boldsymbol{n}_P^f$). However, $\boldsymbol{v}_f = \mathbf{0}$ if and only if $\boldsymbol{v} \wedge \boldsymbol{n}_P^f = \mathbf{0}$. For that reason in the definition of $\boldsymbol{\Psi}_0(P)$, we consider a slightly different, but substantially equivalent, set of homogeneous boundary conditions to that considered in literature.[4,20,43]

Recalling that a sequence is exact if the image of each operator coincides with the kernel of the following one, and that P is contractible, from (2.2) and (2.3) it is easy to check that the following sequence is exact:

$$\mathbb{R} \xrightarrow{\ i\ } \mathbb{P}_{n+2}(P) \xrightarrow{\ \nabla\ } [\mathbb{P}_{n+1}(P)]^3 \xrightarrow{\ \mathbf{curl}\ } [\mathbb{P}_n(P)]^3 \xrightarrow{\ \operatorname{div}\ } \mathbb{P}_{n-1}(P) \xrightarrow{\ 0\ } 0, \tag{2.6}$$

where i denotes the mapping that to every real number r associates the constant function identically equal to r and 0 is the mapping that to every function associates the number 0.

The 3D de Rham complex with minimal regularity (in a contractible domain Ω) is provided by (see for instance Refs. 8 and 37)

$$\mathbb{R} \xrightarrow{\ i\ } H^1(\Omega) \xrightarrow{\ \nabla\ } \boldsymbol{H}(\mathbf{curl}, \Omega) \xrightarrow{\ \mathbf{curl}\ } \boldsymbol{H}(\operatorname{div}, \Omega) \xrightarrow{\ \operatorname{div}\ } L^2(\Omega) \xrightarrow{\ 0\ } 0.$$

In this paper, we consider the de Rham sub-complex with enhanced smoothness[39]

$$\mathbb{R} \xrightarrow{\ i\ } H^1(\Omega) \xrightarrow{\ \nabla\ } \boldsymbol{\Sigma}(\Omega) \xrightarrow{\ \mathbf{curl}\ } [H^1(\Omega)]^3 \xrightarrow{\ \operatorname{div}\ } L^2(\Omega) \xrightarrow{\ 0\ } 0, \tag{2.7}$$

that is suitable for the Stokes (Navier–Stokes) problem. Therefore, our goal is to construct conforming virtual element spaces

$$W_h \subseteq H^1(\Omega), \quad \boldsymbol{\Sigma}_h \subseteq \boldsymbol{\Sigma}(\Omega), \quad \boldsymbol{V}_h \subseteq [H^1(\Omega)]^3, \quad Q_h \subseteq L^2(\Omega) \tag{2.8}$$

that mimic the complex (2.7), i.e. are such that

$$\mathbb{R} \xrightarrow{\ i\ } W_h \xrightarrow{\ \nabla\ } \boldsymbol{\Sigma}_h \xrightarrow{\ \mathbf{curl}\ } \boldsymbol{V}_h \xrightarrow{\ \mathrm{div}\ } Q_h \xrightarrow{\ 0\ } 0 \tag{2.9}$$

is an exact sub-complex of (2.7).

3. The Virtual Element Spaces

This section is devoted to the construction of conforming virtual element spaces (2.8) that compose the virtual sub-complex (2.9). As we will see, the space W_h consists of the lowest degree 3D nodal VEM space,[2,15] whereas the spaces $\boldsymbol{V}_h$ and Q_h (that are the spaces actually used in the discretization of the problem) are the 3D counterparts of the inf-sup stable couple of spaces introduced in Refs. 18 and 57. Therefore, the main novelty of this section is in the construction of the $\boldsymbol{\Sigma}$-conforming space $\boldsymbol{\Sigma}_h$.

In order to facilitate the reading, we present the spaces in the reverse order, from right to left in the sequence (2.9). In particular, in accordance with (2.9), the space $\boldsymbol{\Sigma}_h$ will be carefully designed to fit $\mathbf{curl}\,\boldsymbol{\Sigma}_h \subseteq \boldsymbol{V}_h$.

We stress that the readers mainly interested on the virtual element approximation of the 3D Navier–Stokes equation (and not on the virtual de Rham sequence) can skip Secs. 3.3, 3.4 and 4.

One essential idea in the VEM construction is to define suitable (computable) polynomial projections. For any $n \in \mathbb{N}$ and each polyhedron/face $\mathcal{O}$ we introduce the following polynomial projections:

- the L^2-*projection* $\Pi_n^{0,\mathcal{O}} \colon L^2(\mathcal{O}) \to \mathbb{P}_n(\mathcal{O})$, defined for any $v \in L^2(\mathcal{O})$ by
$$\int_{\mathcal{O}} q_n(v - \Pi_n^{0,\mathcal{O}} v)\mathrm{d}\mathcal{O} = 0 \quad \text{for all } q_n \in \mathbb{P}_n(\mathcal{O}), \tag{3.1}$$
with obvious extension for vector functions $\Pi_n^{0,\mathcal{O}} \colon [L^2(\mathcal{O})]^3 \to [\mathbb{P}_n(\mathcal{O})]^3$, and tensor functions $\boldsymbol{\Pi}_n^{0,\mathcal{O}} \colon [L^2(\mathcal{O})]^{3\times 3} \to [\mathbb{P}_n(\mathcal{O})]^{3\times 3}$,
- the H^1-*seminorm projection* $\Pi_n^{\nabla,\mathcal{O}} \colon H^1(\mathcal{O}) \to \mathbb{P}_n(\mathcal{O})$, defined for any $v \in H^1(\mathcal{O})$ by
$$\begin{cases} \displaystyle\int_{\mathcal{O}} \nabla q_n \cdot \nabla(v - \Pi_n^{\nabla,\mathcal{O}} v)\mathrm{d}\mathcal{O} = 0 \quad \text{for all } q_n \in \mathbb{P}_n(\mathcal{O}), \\ \displaystyle\int_{\partial\mathcal{O}} (v - \Pi_n^{\nabla,\mathcal{O}} v)\mathrm{d}\sigma = 0, \end{cases} \tag{3.2}$$
with obvious extension for vector functions $\Pi_n^{\nabla,\mathcal{O}} \colon [H^1(\mathcal{O})]^3 \to [\mathbb{P}_n(\mathcal{O})]^3$.

Let $k \geq 2$ be the polynomial degree of accuracy of the method. We recall that, in standard finite element fashion, the VEM spaces are first defined elementwise and then assembled globally.

3.1. *Scalar L^2-conforming space*

We start our construction with the rightmost discrete space Q_h in (2.9). Since we are not requiring any smoothness on Q_h, the local space $Q_h(P)$ is simply defined by

$$Q_h(P) := \mathbb{P}_{k-1}(P),$$

having dimension (cf. (2.1)) $\dim(Q_h(P)) = \pi_{k-1,3}$. The corresponding DoFs are chosen, defining for each $q \in Q_h(P)$ the following linear operators

- $\mathbf{D}_Q$**:** the moments up to order $k-1$ of q, i.e.

$$\int_P q p_{k-1} \,\mathrm{d}P \quad \text{for any } p_{k-1} \in \mathbb{P}_{k-1}(P).$$

The global space is given by

$$Q_h := \{q \in L^2(\Omega) \text{ s.t. } q_{|P} \in Q_h(P) \text{ for all } P \in \Omega_h\}. \tag{3.3}$$

It is straightforward to see that the dimension of Q_h is

$$\dim(Q_h) = \pi_{k-1,3} L_P. \tag{3.4}$$

3.2. *Vector H^1-conforming VEM space*

The subsequent space in the de Rham complex (2.9) is the vector-valued H^1-conforming virtual element space $\boldsymbol{V}_h$. The space $\boldsymbol{V}_h$ is a 3D version of the space[18] (see also the guidelines in the appendix of Ref. 17). We make an extensive use of the enhanced technique[2] in order to achieve the computability of the polynomial projections stated in Proposition 5.1.

We first consider on each face f of the element P, the face space

$$\begin{aligned}\widehat{\mathbb{B}}_k(f) := \{&v \in H^1(f) \text{ s.t. (i) } v_{|\partial f} \in C^0(\partial f),\ v_{|e} \in \mathbb{P}_k(e) \text{ for all } e \in \partial f,\\ &\text{(ii) } \Delta_f v \in \mathbb{P}_{k+1}(f),\\ &\text{(iii) } (v - \Pi_k^{\nabla,f} v, \widehat{p}_{k+1})_f = 0 \text{ for all } \widehat{p}_{k+1} \in \widehat{\mathbb{P}}_{k+1\setminus k-2}(f)\}\end{aligned} \tag{3.5}$$

and the boundary space

$$\widehat{\mathbb{B}}_k(\partial P) := \{v \in C^0(\partial P) \text{ such that } v_{|f} \in \widehat{\mathbb{B}}_k(f) \text{ for any } f \in \partial P\}$$

that is a modification of the standard boundary nodal VEM.[13] Indeed the "super-enhanced" constraints (condition iii) in the definition (3.5)) are needed to exactly compute the polynomial projection $\Pi^{0,f}_{k+1}$ (see Proposition 5.1).

On the polyhedron P we first define the virtual element space $\widetilde{\boldsymbol{V}}_h(P)$

$$\begin{aligned}\widetilde{\boldsymbol{V}}_h(P) := \{&\boldsymbol{v} \in [H^1(P)]^3 \text{ s.t. (i) } \boldsymbol{v}_{|\partial P} \in [\widehat{\mathbb{B}}_k(\partial P)]^3,\\ &\text{(ii) } \boldsymbol{\Delta v} + \nabla s \in \boldsymbol{x} \wedge [\mathbb{P}_{k-1}(P)]^3 \text{ for some } s \in L^2_0(P),\\ &\text{(iii) } \operatorname{div} \boldsymbol{v} \in \mathbb{P}_{k-1}(P)\},\end{aligned} \tag{3.6}$$

and afterwards our velocity space

$$\boldsymbol{V}_h(P) := \{\boldsymbol{v} \in \widetilde{\boldsymbol{V}}_h(P) \text{ s.t. } (\boldsymbol{v} - \Pi_k^{\nabla,P}\boldsymbol{v},\, \boldsymbol{x} \wedge \widehat{\boldsymbol{p}}_{k-1})_P = 0 \quad \text{for all } \widehat{\boldsymbol{p}}_{k-1} \in [\widehat{\mathbb{P}}_{k-1\setminus k-3}(P)]^3\}. \tag{3.7}$$

The definition above is the 3D counterpart of the virtual elements,[18] in particular we remark that the enhancing constraints in definition (3.7) are necessary to achieve the computability of the L^2-projection $\Pi_k^{0,P}$ (see Proposition 5.1). Moreover, notice that the space $\boldsymbol{V}_h(P)$ contains $[\mathbb{P}_k(P)]^3$ and this will guarantee the good approximation property of the space (cf. Theorem 5.1).

Proposition 3.1. *The dimension of* $\boldsymbol{V}_h(P)$ *is given by*

$$\dim(\boldsymbol{V}_h(P)) = 3\ell_V + 3(k-1)\ell_e + 3\pi_{k-2,2}\ell_f + 3\pi_{k-2,3}.$$

Moreover, the following linear operators $\mathbf{D}_{\boldsymbol{V}}$ *split into five subsets constitute a set of DoFs for* $\boldsymbol{V}_h(P)$:

- $\mathbf{D^1}_{\boldsymbol{V}}$**:** *the values of* $\boldsymbol{v}$ *at the vertexes of* P,
- $\mathbf{D^2}_{\boldsymbol{V}}$**:** *the values of* $\boldsymbol{v}$ *at* $k-1$ *distinct points of every edge* e *of* P,
- $\mathbf{D^3}_{\boldsymbol{V}}$**:** *the face moments of* $\boldsymbol{v}$ (*split into normal and tangential components*)

$$\int_f (\boldsymbol{v} \cdot \boldsymbol{n}_P^f) p_{k-2}\,\mathrm{d}f, \quad \int_f \boldsymbol{v}_\tau \cdot \boldsymbol{p}_{k-2}\,\mathrm{d}f,$$

  for all $p_{k-2} \in \mathbb{P}_{k-2}(f)$ *and* $\boldsymbol{p}_{k-2} \in [\mathbb{P}_{k-2}(f)]^2$,
- $\mathbf{D^4}_{\boldsymbol{V}}$**:** *the volume moments of* $\boldsymbol{v}$

$$\int_P \boldsymbol{v} \cdot (\boldsymbol{x} \wedge \boldsymbol{p}_{k-3})\mathrm{d}P \quad \textit{for all } \boldsymbol{p}_{k-3} \in [\mathbb{P}_{k-3}(P)]^3,$$

- $\mathbf{D^5}_{\boldsymbol{V}}$**:** *the volume moments of* $\operatorname{div}\boldsymbol{v}$

$$\int_P (\operatorname{div}\boldsymbol{v})\widehat{p}_{k-1}\,\mathrm{d}P \quad \textit{for all } \widehat{p}_{k-1} \in \widehat{\mathbb{P}}_{k-1\setminus 0}(P).$$

Proof. We only sketch the proof since it follows the guidelines of Proposition 3.1 in Ref. 57 for the analogous 2D space. First of all, recalling (2.1) and polynomial decomposition (2.2), simple computations yield

$$\begin{gathered}\#\mathbf{D^1}_{\boldsymbol{V}} = 3\ell_V, \quad \#\mathbf{D^2}_{\boldsymbol{V}} = 3(k-1)\ell_e, \quad \#\mathbf{D^3}_{\boldsymbol{V}} = 3\pi_{k-2,2}\ell_f, \\ \#\mathbf{D^4}_{\boldsymbol{V}} = 3\pi_{k-2,3} - \pi_{k-1,3} + 1, \quad \#\mathbf{D^5}_{\boldsymbol{V}} = \pi_{k-1,3} - 1,\end{gathered} \tag{3.8}$$

and therefore

$$\#\mathbf{D}_{\boldsymbol{V}} = 3\ell_V + 3(k-1)\ell_e + 3\pi_{k-2,2}\ell_f + 3\pi_{k-2,3}.$$

Now employing Proposition 2 and Remark 5 in Ref. 2, it can be shown that the DoFs $\mathbf{D^1}_{\boldsymbol{V}}$, $\mathbf{D^2}_{\boldsymbol{V}}$, $\mathbf{D^3}_{\boldsymbol{V}}$ are unisolvent for the space $[\widehat{\mathbb{B}}_k(\partial P)]^3$. Therefore, it holds that

$$\dim([\widehat{\mathbb{B}}_k(\partial P)]^3) = 3\ell_V + 3(k-1)\ell_e + 3\pi_{k-2,2}\ell_f, \tag{3.9}$$

which in turn implies (recalling (3.6) and (3.7))

$$\dim(\boldsymbol{V}_h(P)) \geq \#\mathbf{D}_{\boldsymbol{V}}.$$

Now the result follows by proving that $\mathbf{D}_{\boldsymbol{V}}(\boldsymbol{v}) = \mathbf{0}$ implies that $\boldsymbol{v}$ is identically zero, which can be easily shown first working on ∂P and then inside P. As a consequence the linear operators $\mathbf{D}_{\boldsymbol{V}}$ are unisolvent for $\boldsymbol{V}_h$ and in particular $\dim(\boldsymbol{V}_h(P)) = \#\mathbf{D}_{\boldsymbol{V}}$. □

The global space $\boldsymbol{V}_h$ is defined by gluing the local spaces with the obvious associated sets of global DoFs:

$$\boldsymbol{V}_h := \{\boldsymbol{v} \in [H^1(\Omega)]^3 \text{ s.t. } \boldsymbol{v}_{|P} \in \boldsymbol{V}_h(P) \text{ for all } P \in \Omega_h\}. \tag{3.10}$$

The dimension of $\boldsymbol{V}_h$ is given by

$$\dim(\boldsymbol{V}_h) = 3L_V + 3(k-1)L_e + 3\pi_{k-2,2}L_f + 3\pi_{k-2,3}L_P. \tag{3.11}$$

We also consider the discrete kernel

$$\boldsymbol{Z}_h := \left\{\boldsymbol{v} \in \boldsymbol{V}_h \text{ s.t. } \int_\Omega \operatorname{div} \boldsymbol{v}\, q \,\mathrm{d}\Omega = 0 \text{ for all } q \in Q_h\right\}, \tag{3.12}$$

and the local version

$$\boldsymbol{Z}_h(P) := \left\{\boldsymbol{v} \in \boldsymbol{V}_h(P) \text{ s.t. } \int_P \operatorname{div} \boldsymbol{v}\, q \,\mathrm{dP} = 0 \text{ for all } q \in Q_h(P)\right\}.$$

A crucial observation is that, extending to the 3D case the result in Ref. 17, the proposed discrete pressure space (3.3) and the H^1-conforming velocity space (3.10) are such that $\operatorname{div} \boldsymbol{V}_h \subseteq Q_h$. As a consequence the crucial kernel inclusion holds

$$\boldsymbol{Z}_h \subseteq \boldsymbol{Z}. \tag{3.13}$$

The inclusion here above and explicit computations (cf. (3.8)) yield that

$$\dim(\boldsymbol{Z}_h) = 3L_V + 3(k-1)L_e + 3\pi_{k-2,2}L_f + (3\pi_{k-2,3} - \pi_{k-1,3})N_P.$$

Property (3.13) has several important advantages, as explored in Refs. 18, 46 and 48.

Remark 3.1. In definition (3.7) the H^1-seminorm projection $\Pi_k^{\nabla,P}$ can be actually replaced by any polynomial projection Π_k^P that is computable on the basis of the DoFs $\mathbf{D}_{\boldsymbol{V}}$ (in the sense of Proposition 5.1). This change clearly propagates throughout the rest of the analysis (see definitions (3.17) and (3.27)). An analogous observation holds also for the operator $\Pi_k^{\nabla,f}$ in condition (iii) of definition (3.5). This remark allows to make use of computationally cheaper projections, as done in the numerical tests of Sec. 6.

3.3. *Vector $\boldsymbol{\Sigma}$-conforming VEM space*

In this subsection, we consider the construction of the $\boldsymbol{\Sigma}$-conforming virtual space $\boldsymbol{\Sigma}_h$ in (2.9). As mentioned before, this brick constitutes the main novelty in the

construction of the virtual de Rham sequence (2.9), that is carefully designed to satisfy $\mathbf{curl}\,\boldsymbol{\Sigma}_h = \boldsymbol{Z}_h$.

We start by introducing on each face $f \in \partial P$ the face space

$$\begin{aligned}\boldsymbol{S}_k(f) := \{\boldsymbol{\sigma} \in \boldsymbol{H}(\mathrm{div}_f, f) \cap \boldsymbol{H}(\mathrm{rot}_f, f) \text{ s.t. (i) } (\boldsymbol{\sigma}\cdot\boldsymbol{t}_e)_{|e} \in \mathbb{P}_0(e), \quad \forall e \in \partial f,\\ \text{(ii) } \mathrm{div}_f\boldsymbol{\sigma} = 0,\ \text{(iii) } \mathrm{rot}_f\boldsymbol{\sigma} \in \widehat{\mathbb{B}}_k(f)\},\end{aligned} \tag{3.14}$$

and the boundary space

$$\begin{aligned}\boldsymbol{S}_k(\partial P) := \{\boldsymbol{\sigma} \in [L^2(\partial P)]^3 \text{ s.t. } \boldsymbol{\sigma}_\tau \in \boldsymbol{S}_k(f) \text{ for any } f \in \partial P,\\ (\boldsymbol{\sigma}_{f_1}\cdot\boldsymbol{t}_e)_{|e} = (\boldsymbol{\sigma}_{f_2}\cdot\boldsymbol{t}_e)_{|e},\ \forall e \subseteq \partial f_1 \cap \partial f_2,\ f_1, f_2 \in \partial P\}.\end{aligned} \tag{3.15}$$

We recall that the differential problem in definition (3.14) posed on the simply connected face f is well posed if and only if the prescribed problem data satisfy the compatibility condition (2.5).

On the polyhedron P we first define the enlarged virtual space:

$$\begin{aligned}\widetilde{\boldsymbol{\Sigma}}_h(P) := \Big\{&\boldsymbol{\varphi} \in \boldsymbol{\Psi}(P) \text{ s.t. (i) } \boldsymbol{\varphi}_{|\partial P} \in \boldsymbol{S}_k(\partial P),\ \int_{\partial P} \boldsymbol{\varphi}\cdot\boldsymbol{n}_P\,\mathrm{d}f = 0,\\ &\text{(ii) } (\mathbf{curl}\,\boldsymbol{\varphi})_{|\partial P} \in [\widehat{\mathbb{B}}_k(\partial P)]^3,\\ &\text{(iii) } \int_P \boldsymbol{\Delta}\,\boldsymbol{\varphi}\cdot\boldsymbol{\Delta}\,\boldsymbol{\psi}\,\mathrm{d}P = \int_P \widetilde{\boldsymbol{p}}_{k-1}\cdot\boldsymbol{\psi}\,\mathrm{d}P,\ \forall\boldsymbol{\psi} \in \boldsymbol{\Psi}_0(P),\\ &\text{for some } \widetilde{\boldsymbol{p}}_{k-1} \in [\mathbb{P}_{k-1}(P)]^3 \cap \boldsymbol{Z}(P)\Big\},\end{aligned} \tag{3.16}$$

and afterwards the final space

$$\begin{aligned}\boldsymbol{\Sigma}_h(P) := \{\boldsymbol{\varphi} \in \widetilde{\boldsymbol{\Sigma}}_h(P) \text{ s.t. } (\mathbf{curl}\,\boldsymbol{\varphi} - \Pi_k^{\nabla,P}\mathbf{curl}\,\boldsymbol{\varphi},\, \boldsymbol{x}\wedge\widehat{\boldsymbol{p}}_{k-1})_P = 0\\ \text{for all } \widehat{\boldsymbol{p}}_{k-1} \in [\widehat{\mathbb{P}}_{k-1\setminus k-3}(P)]^3\}.\end{aligned} \tag{3.17}$$

We address the well-posedness of the biharmonic problem in definition (3.16) in Appendix A. Note that, in accordance with the target $\mathbf{curl}\,\boldsymbol{\Sigma}_h \subseteq \boldsymbol{V}_h$ (respectively, $\mathbf{curl}\,\widetilde{\boldsymbol{\Sigma}}_h \subseteq \widetilde{\boldsymbol{V}}_h$) the enhanced constraints in (3.17) are the **curl** version of those in (3.7) and (ii) in definition (3.16) corresponds to (i) in (3.6). Whereas we will see that **curl** of the solutions of the biharmonic problem (iii) in (3.16) are solutions to the Stokes problem (ii)–(iii) in (3.6) (see Proposition 4.2).

Proposition 3.2. *The dimension of* $\boldsymbol{\Sigma}_h(P)$ *is given by*

$$\dim(\boldsymbol{\Sigma}_h(P)) = 3\ell_V + (3k-2)\ell_e + (3\pi_{k-2,2}-1)\ell_f + 3\pi_{k-2,3} - \pi_{k-1,3} + 1.$$

Moreover, the following linear operators $\mathbf{D}_{\boldsymbol{\Sigma}}$ *constitute a set of DoFs for* $\boldsymbol{\Sigma}_h(P)$ *namely*:

- $\mathbf{D^1_\Sigma}$**:** *the values of* $\mathbf{curl}\,\boldsymbol{\varphi}$ *at the vertexes of* P,
- $\mathbf{D^2_\Sigma}$**:** *the values of* $\mathbf{curl}\,\boldsymbol{\varphi}$ *at* $k-1$ *distinct points of every edge* e *of* P,

- $\mathbf{D^3_\Sigma}$: *the face moments of* $\mathbf{curl}\,\boldsymbol{\varphi}$ (*split into normal and tangential components*)

$$\int_f (\mathbf{curl}\,\boldsymbol{\varphi}\cdot\boldsymbol{n}_P^f)\widehat{p}_{k-2}\,\mathrm{d}f \quad \textit{for all } \widehat{p}_{k-2}\in\widehat{\mathbb{P}}_{k-2\setminus 0}(f),$$

$$\int_f (\mathbf{curl}\,\boldsymbol{\varphi})_\tau\cdot\boldsymbol{p}_{k-2}\,\mathrm{d}f \quad \textit{for all } \boldsymbol{p}_{k-2}\in[\mathbb{P}_{k-2}(f)]^2,$$

- $\mathbf{D^4_\Sigma}$: *the volume moments of* $\mathbf{curl}\,\boldsymbol{\varphi}$

$$\int_P \mathbf{curl}\,\boldsymbol{\varphi}\cdot(\boldsymbol{x}\wedge\boldsymbol{p}_{k-3})\mathrm{d}P \quad \textit{for all } \boldsymbol{p}_{k-3}\in[\mathbb{P}_{k-3}(P)]^3,$$

- $\mathbf{D^5_\Sigma}$: *the edge mean value of* $\boldsymbol{\varphi}\cdot\boldsymbol{t}_e$, *i.e.*

$$\frac{1}{|e|}\int_e \boldsymbol{\varphi}\cdot\boldsymbol{t}_e\,\mathrm{d}s.$$

Proof. We prove that the linear operators $\mathbf{D_\Sigma}$ plus the additional moments

$$\widetilde{\mathbf{D}}^{\mathbf{4}}_{\boldsymbol{\Sigma}}\colon \int_P \mathbf{curl}\,\boldsymbol{\varphi}\cdot(\boldsymbol{x}\wedge\widehat{\boldsymbol{p}}_{k-1})\mathrm{d}P \quad \text{for all } \widehat{\boldsymbol{p}}_{k-1}\in[\widehat{\mathbb{P}}_{k-1\setminus k-3}(P)]^3,$$

constitute a set of DoFs for the enlarged space $\widetilde{\boldsymbol{\Sigma}}_h(P)$ in (3.16). Once the proof for $\widetilde{\boldsymbol{\Sigma}}_h(P)$ is given, the extension to the smaller space $\boldsymbol{\Sigma}_h(P)$ easily follows by employing standard techniques for VEM enhanced spaces (see Ref. 2 and Proposition 5.1 in Ref. 19). We preliminary observe that $\mathbf{D^4_\Sigma}+\widetilde{\mathbf{D}}^{\mathbf{4}}_{\boldsymbol{\Sigma}}$ are equivalent to prescribe the moments $\int_P \mathbf{curl}\,\boldsymbol{\varphi}\cdot(\boldsymbol{x}\wedge\boldsymbol{p}_{k-1})\mathrm{d}P$ for all $\boldsymbol{p}_{k-1}\in[\mathbb{P}_{k-1}(P)]^3$.

We start the proof counting the number of the linear operators $\widetilde{\mathbf{D}}_{\boldsymbol{\Sigma}}=\mathbf{D_\Sigma}+\widetilde{\mathbf{D}}^{\mathbf{4}}_{\boldsymbol{\Sigma}}$. Using similar computations as in (3.8) we have

$$\#\mathbf{D^1_\Sigma}=3\ell_V,\quad \#\mathbf{D^2_\Sigma}=3(k-1)\ell_e,\quad \#\mathbf{D^3_\Sigma}=(3\pi_{k-2,2}-1)\ell_f,$$
$$\#\mathbf{D^4_\Sigma}+\#\widetilde{\mathbf{D}}^{\mathbf{4}}_{\boldsymbol{\Sigma}}=3\pi_{k,3}-\pi_{k+1,3}+1,\quad \#\mathbf{D^5_\Sigma}=\ell_e,$$

and thus

$$\#\widetilde{\mathbf{D}}_{\boldsymbol{\Sigma}}=3\ell_V+(3k-2)\ell_e+(3\pi_{k-2,2}-1)\ell_f+3\pi_{k,3}-\pi_{k+1,3}+1. \tag{3.18}$$

Employing Theorem A.1, given $\widetilde{\boldsymbol{p}}_{k-1}\in[\mathbb{P}_{k-1}(P)]^3\cap\boldsymbol{Z}(P)$, $\boldsymbol{g}\in[\widehat{\mathbb{B}}_k(\partial P)]^3$ and $\boldsymbol{h}\in\boldsymbol{S}_k(\partial P)$ satisfying the compatibility condition (cf. (2.4)) $\boldsymbol{g}\cdot\boldsymbol{n}_P^f=\mathrm{rot}_f\,\boldsymbol{h}_\tau$ on any $f\in\partial P$, there exists a unique function $\boldsymbol{\varphi}\in\boldsymbol{\Psi}(P)$ such that

$$\begin{cases}\displaystyle\int_P \boldsymbol{\Delta}\,\boldsymbol{\varphi}\cdot\boldsymbol{\Delta}\,\boldsymbol{\psi}\,\mathrm{d}P=\int_P\widetilde{\boldsymbol{p}}_{k-1}\cdot\boldsymbol{\psi}\,\mathrm{d}P & \text{for all } \boldsymbol{\psi}\in\boldsymbol{\Psi}_0(P),\\ \displaystyle\int_{\partial P}\boldsymbol{\varphi}\cdot\boldsymbol{n}_P\,\mathrm{d}f=0,\\ \boldsymbol{\varphi}_\tau=\boldsymbol{h}_\tau & \text{on } \partial P,\\ \mathbf{curl}\,\boldsymbol{\varphi}=\boldsymbol{g} & \text{on } \partial P.\end{cases}$$

Therefore,

$$\dim(\widetilde{\boldsymbol{\Sigma}}_h(P)) = \dim([\mathbb{P}_{k-1}(P)]^3 \cap \boldsymbol{Z}(P)) + \dim([\widehat{\mathbb{B}}_k(\partial P)]^3) + \dim(\boldsymbol{S}_k(\partial P)) - \dim(\widehat{\mathbb{B}}_k(f))\ell_f, \quad (3.19)$$

where the last term $(-\dim(\widehat{\mathbb{B}}_k(f))\ell_f)$ ensues from the compatibility condition among $\boldsymbol{h}$ and $\boldsymbol{g}$ mentioned above. We calculate the addenda in the right-hand side of (3.19). Regarding the first term in (3.19), we preliminary note that the following characterization ensues from the exact sequence (2.6) and polynomial decomposition (2.2)

$$[\mathbb{P}_{k-1}(P)]^3 \cap \boldsymbol{Z}(P) = \mathbf{curl}([\mathbb{P}_k(P)]^3) = \mathbf{curl}(\boldsymbol{x} \wedge [\mathbb{P}_{k-1}(P)]^3). \quad (3.20)$$

Employing again the exact sequence (2.6), **curl** restricted to $(\boldsymbol{x} \wedge [\mathbb{P}_{k-1}(P)]^3)$ is actually an isomorphism, therefore from (3.20) and (3.8) it follows that

$$\dim([\mathbb{P}_{k-1}(P)]^3 \cap \boldsymbol{Z}(P)) = \dim(\boldsymbol{x} \wedge [\mathbb{P}_{k-1}(P)]^3) = 3\pi_{k,3} - \pi_{k+1,3} + 1. \quad (3.21)$$

From definitions (3.14) and (3.15), direct computations yield

$$\dim(\boldsymbol{S}_k(\partial P)) = \ell_e + (\dim(\widehat{\mathbb{B}}_k(f)) - 1)\ell_f, \quad (3.22)$$

where the -1 in the formula above is due to the compatibility condition (2.5).

Collecting (3.21), (3.9) and (3.22) in (3.19) (compare with (3.18)) we get

$$\dim(\widetilde{\boldsymbol{\Sigma}}_h(P)) = \#\widetilde{\mathbf{D}}_{\boldsymbol{\Sigma}}.$$

Having proved that $\#\widetilde{\mathbf{D}}_{\boldsymbol{\Sigma}}$ is equal to $\dim(\widetilde{\boldsymbol{\Sigma}}_h(P))$, in order to validate that the linear operators $\widetilde{\mathbf{D}}_{\boldsymbol{\Sigma}}$ constitute a set of DoFs for $\widetilde{\boldsymbol{\Sigma}}_h(P)$ we have to check that they are unisolvent. Let $\boldsymbol{\varphi} \in \widetilde{\boldsymbol{\Sigma}}_h(P)$ such that $\widetilde{\mathbf{D}}_{\boldsymbol{\Sigma}}(\boldsymbol{\varphi}) = \mathbf{0}$, we need to show that $\boldsymbol{\varphi}$ is identically zero. It is straightforward that $\mathbf{D^1}_{\boldsymbol{\Sigma}}(\boldsymbol{\varphi}) = \mathbf{D^2}_{\boldsymbol{\Sigma}}(\boldsymbol{\varphi}) = \mathbf{0}$ implies

$$(\mathbf{curl}\,\boldsymbol{\varphi})_{|\partial f} = \mathbf{0} \quad \text{for any } f \in \partial P. \quad (3.23)$$

Recalling the well-known results for nodal boundary spaces,[13] it is quite obvious to check that (3.23) $\mathbf{D^3}_{\boldsymbol{\Sigma}}(\boldsymbol{\varphi}) = \mathbf{0}$ implies

$$(\mathbf{curl}\,\boldsymbol{\varphi})_f = \mathbf{0} \quad \text{for any } f \in \partial P.$$

In order to get also the normal component of $(\mathbf{curl}\,\boldsymbol{\varphi})_{|f}$ equal to zero, based on $\mathbf{D^3}_{\boldsymbol{\Sigma}}(\boldsymbol{\varphi}) = \mathbf{0}$, it is sufficient to observe that the compatibility conditions (2.4) and (2.5) give

$$\int_f \mathbf{curl}\,\boldsymbol{\varphi} \cdot \boldsymbol{n}_P^f \,\mathrm{d}f = \int_f \mathrm{rot}_f\, \boldsymbol{\varphi}_\tau \,\mathrm{d}f = \int_{\partial f} \boldsymbol{\varphi} \cdot \boldsymbol{t}_f \,\mathrm{d}s = \sum_{e \in \partial f} \int_e \boldsymbol{\varphi} \cdot \boldsymbol{t}_f^e \,\mathrm{d}s = \sum_{e \in \partial f} |e|\, \mathbf{D^5}_{\boldsymbol{\Sigma},e}(\boldsymbol{\varphi}) \boldsymbol{t}_e \cdot \boldsymbol{t}_f^e \quad \text{for any } f \in \partial P \quad (3.24)$$

that is equal to 0 since $\mathbf{D^5_\Sigma}(\boldsymbol{\varphi}) = \mathbf{0}$. Therefore, we have proved that

$$\mathbf{curl}\,\boldsymbol{\varphi} = \mathbf{0} \quad \text{on } \partial P. \tag{3.25}$$

Moreover, being $\mathbf{D^5_\Sigma}(\boldsymbol{\varphi}) = \mathbf{0}$, from (3.25) and (2.4) and definition (3.14) for any $f \in \partial P$ we infer

$$(\boldsymbol{\varphi}_f \cdot \boldsymbol{t}_e)_{|e} = 0 \quad \text{for any } e \in \partial f, \quad \mathrm{div}_f\, \boldsymbol{\varphi}_\tau = 0 \quad \text{and} \quad \mathrm{rot}_f\, \boldsymbol{\varphi}_\tau = 0 \quad \text{on } f,$$

and thus we obtain

$$\boldsymbol{\varphi}_\tau = \mathbf{0} \quad \text{for any } f \in \partial P. \tag{3.26}$$

Finally, by definition of $\widetilde{\boldsymbol{\Sigma}}_h(P)$, there exists $\widetilde{\boldsymbol{p}}_{k-1} \in [\mathbb{P}_{k-1}(P)]^3 \cap \boldsymbol{Z}(P)$ such that

$$\int_P \boldsymbol{\Delta}\,\boldsymbol{\varphi} \cdot \boldsymbol{\Delta}\,\boldsymbol{\psi}\,\mathrm{d}P = \int_P \widetilde{\boldsymbol{p}}_{k-1} \cdot \boldsymbol{\psi}\,\mathrm{d}P \quad \text{for all } \boldsymbol{\psi} \in \boldsymbol{\Psi}_0(P).$$

Therefore, being $\boldsymbol{\varphi} \in \boldsymbol{\Psi}_0(P)$ (cf. (3.25) and (3.26)) we infer

$$\begin{aligned}
\|\boldsymbol{\Delta}\,\boldsymbol{\varphi}\|^2_{0,P} &= \int_P \boldsymbol{\Delta}\,\boldsymbol{\varphi} \cdot \boldsymbol{\Delta}\,\boldsymbol{\varphi}\,\mathrm{d}P = \int_P \widetilde{\boldsymbol{p}}_{k-1} \cdot \boldsymbol{\varphi}\,\mathrm{d}P \\
&= \int_P \mathbf{curl}\,(\boldsymbol{x} \wedge \boldsymbol{q}_{k-1}) \cdot \boldsymbol{\varphi}\,\mathrm{d}P \qquad \text{(characterization (3.20))} \\
&= \int_P \boldsymbol{x} \wedge \boldsymbol{q}_{k-1} \cdot \mathbf{curl}\,\boldsymbol{\varphi}\,\mathrm{d}P \qquad \text{(integration by parts + (3.26))}
\end{aligned}$$

and thus, since $\mathbf{D^4_\Sigma}(\boldsymbol{\varphi})$ and $\widetilde{\mathbf{D}}^{\mathbf{4}}_{\boldsymbol{\Sigma}}(\boldsymbol{\varphi})$ are 0, we obtain $\|\boldsymbol{\Delta}\,\boldsymbol{\varphi}\|^2_{0,P} = 0$. Now the proof follows by the fact that $\|\boldsymbol{\Delta}\cdot\|_{0,P}$ is a norm on $\boldsymbol{\Psi}_0(P)$ (see Lemma 5.2 in Ref. 43 and (A.1)). □

Notice that the DoFs $\mathbf{D_\Sigma}$ are conveniently chosen in order to have a direct correspondence between the **curl** of the Lagrange-type basis functions of $\boldsymbol{\Sigma}_h$ and the Lagrange basis functions of $\boldsymbol{V}_h$.

Remark 3.2. A careful inspection of Theorem A.1 (see also Remark 5.1 in Ref. 43 and Ref. 20) reveals that the space (3.17) admits the equivalent formulation

$$\begin{aligned}
\boldsymbol{\Sigma}_h(P) := \{&\boldsymbol{\varphi} \in \boldsymbol{\Psi}(P) \text{ s.t. (i) } \boldsymbol{\varphi}_{|\partial P} \in \boldsymbol{S}_k(\partial P),\ \text{(ii) } (\mathbf{curl}\,\boldsymbol{\varphi})_{|\partial P} \in [\widehat{\mathbb{B}}_k(\partial P)]^3, \\
&\text{(iii) } \boldsymbol{\Delta}^2\,\boldsymbol{\varphi} \in [\mathbb{P}_{k-1}(P)]^3 \cap \boldsymbol{Z}(P),\ \text{(iv) } \mathrm{div}\,\boldsymbol{\varphi} = 0, \\
&\text{(v) } (\mathbf{curl}\,\boldsymbol{\varphi} - \Pi^{\nabla,P}_k \mathbf{curl}\,\boldsymbol{\varphi},\, \boldsymbol{x} \wedge \widehat{\boldsymbol{p}}_{k-1})_P = 0,\ \forall\, \widehat{\boldsymbol{p}}_{k-1} \in [\widehat{\mathbb{P}}_{k-1\setminus k-3}(P)]^3\}.
\end{aligned} \tag{3.27}$$

The global space $\boldsymbol{\Sigma}_h$ is defined by collecting the local spaces $\boldsymbol{\Sigma}_h(P)$, i.e.

$$\boldsymbol{\Sigma}_h := \{\boldsymbol{\varphi} \in \boldsymbol{\Sigma}(\Omega) \text{ s.t. } \boldsymbol{\varphi}_{|P} \in \boldsymbol{\Sigma}_h(P) \text{ for all } P \in \Omega_h\}. \tag{3.28}$$

The global set of DoFs is the global counterpart of $\mathbf{D_\Sigma}$, in particular the choice of DoFs $\mathbf{D_\Sigma}$ establishes the conforming property $\mathbf{curl}\,\boldsymbol{\Sigma}_h \subseteq [H^1(\Omega)]^3$. The dimension of $\boldsymbol{\Sigma}_h$ is given by

$$\dim(\boldsymbol{\Sigma}_h) = 3L_V + (3k-2)L_e + (3\pi_{k-2,2} - 1)L_f + (3\pi_{k-2,3} - \pi_{k-1,3} + 1)L_P.$$

3.4. *Scalar H^1-conforming VEM space*

In this section, we briefly define the H^1-conforming space W_h in the virtual complex (2.9). The space W_h consists of low-order nodal VEM.[13]

We first introduce the low-order boundary space

$$\mathbb{B}_1(f) := \{v \in H^1(f) \text{ s.t. } v_{|\partial f} \in C(\partial f),\ v_{|e} \in \mathbb{P}_1(e) \text{ for all } e \in \partial f,\ \Delta_f v = 0\}, \tag{3.29}$$

and then we consider the VEM space on the polyhedron P

$$W_h(P) := \{v \in H^1(P) \text{ s.t. } v_{|\partial P} \in C^0(\partial P),\ v_{|f} \in \mathbb{B}_1(f)\ \forall\, f \in \partial P,\ \Delta v = 0\}, \tag{3.30}$$

with the associated set of DoFs:

- $\mathbf{D}_W$**:** the values of v at the vertexes of the polyhedron P.

It is straightforward to see that the dimension of $W_h(P)$ is $\dim(W_h(P)) = \ell_V$.

The global space is obtained by collecting the local spaces

$$W_h := \{v \in H^1(\Omega) \text{ s.t. } v_{|P} \in W_h(P) \text{ for all } P \in \Omega_h\} \tag{3.31}$$

with the obviously associated DoFs. The dimension of W_h is given by $\dim(W_h) = L_V$.

4. The Virtual Elements de Rham Sequence

The aim of this section is to show that the set of virtual spaces introduced in Sec. 3 realizes the exact sequence (2.9).

Theorem 4.1. *The sequence* (2.9) *constitutes an exact complex.*

The theorem follows by Propositions 4.1–4.3, here below, stating that the image of each operator in (2.9) coincides with the kernel of the following one.

Proposition 4.1. *Let W_h and $\boldsymbol{\Sigma}_h$ be the spaces defined in* (3.31) *and* (3.28)*, respectively. Then*

$$\nabla W_h = \{\boldsymbol{\varphi} \in \boldsymbol{\Sigma}_h \text{ s.t. } \mathbf{curl}\,\boldsymbol{\varphi} = \mathbf{0} \text{ in } \Omega\}.$$

Proof. Essentially we need to prove that

(*i*1) for every $w \in W_h$, $\nabla w \in \boldsymbol{\Sigma}_h$ and $\mathbf{curl}(\nabla w) = \mathbf{0}$,
(*i*2) for every $\boldsymbol{\varphi} \in \boldsymbol{\Sigma}_h$ with $\mathbf{curl}\,\boldsymbol{\varphi} = \mathbf{0}$, there exists $w \in W_h$ such that $\nabla w = \boldsymbol{\varphi}$.

For what concerns the inclusion **(*i*1)**, every $w \in W_h$ clearly satisfies $\mathbf{curl}(\nabla w) = \mathbf{0} \in [H^1(\Omega)]^3$, therefore we need to verify that $(\nabla w)_{|P} \in \boldsymbol{\Sigma}_h(P)$ for any $P \in \Omega_h$. Notice that the tangential component of ∇w satisfies

$$(\nabla\, w)_\tau = \nabla_f w_\tau \quad \text{on each face } f \in \partial P. \tag{4.1}$$

From definition (3.29) and (3.14), for any $f \in \partial P$ we infer

$$\begin{aligned}
&\text{(i)} \quad (\nabla w \cdot \boldsymbol{t}_e)_{|e} = \frac{\partial w}{\partial \boldsymbol{t}_e} \in \mathbb{P}_0(e), \quad \forall\, e \in \partial f, && (w_{|e} \in \mathbb{P}_1(e)),\\
&\text{(ii)} \quad \mathrm{div}_f(\nabla_f w_\tau) = 0 \quad \text{in } f && (\Delta_f\, w_\tau = 0),\\
&\text{(iii)} \quad \mathrm{rot}_f(\nabla_f w_\tau) = 0 \quad \text{in } f && \text{(vector calculus identity)}
\end{aligned}$$

that, recalling (4.1), implies $(\nabla w)_\tau \in \boldsymbol{S}_k(f)$. Moreover, $w \in C^0(\partial P)$ entails

$$[(\nabla w)_{f_1} \cdot \boldsymbol{t}_e]_{|e} = [(\nabla w)_{f_2} \cdot \boldsymbol{t}_e]_{|e} \quad \text{for any } e \subseteq \partial f_1 \cap f_2,$$

and thus (cf. definition (3.15))

$$(\nabla w)_{|\partial P} \in \boldsymbol{S}_k(\partial P). \tag{4.2}$$

Furthermore, definition (3.30) implies

$$\begin{aligned}
&\text{(i)} \quad \int_{\partial P} \nabla w \cdot \boldsymbol{n}_P \,\mathrm{d}f = \int_P \Delta w \,\mathrm{d}P = 0, && (\text{div. theorem} + \Delta w = 0),\\
&\text{(ii)} \quad \mathbf{curl}(\nabla w) = \mathbf{0} \quad \text{in } \overline{P} && \text{(vector calculus identity)},\\
&\text{(iii)} \quad \boldsymbol{\Delta}(\nabla w) = \boldsymbol{\nabla}(\Delta w) = \mathbf{0} \quad \text{in } P && (\Delta\, w = 0).
\end{aligned} \tag{4.3}$$

Collecting (4.2) and (4.3) in definition (3.17), we easily obtain ***(i1)***.

We prove now the property ***(i2)***. Consider $\boldsymbol{\varphi} \in \boldsymbol{\Sigma}_h$ such that $\mathbf{curl}\,\boldsymbol{\varphi} = \mathbf{0}$. Since (2.7) is an exact sequence, there exists unique (up to constant) $\widetilde{w} \in H^1(\Omega)$ such that $\nabla\,\widetilde{w} = \boldsymbol{\varphi}$. Therefore, for any face f in the decomposition Ω_h, the tangential component of $\nabla\widetilde{w}$ satisfies (cf. definition (3.14))

$$(\nabla\widetilde{w})_\tau = \nabla_f \widetilde{w}_\tau = \boldsymbol{\varphi}_\tau \in [L^2(f)]^2 \quad \text{on } f.$$

Hence on each face f the function $\widetilde{w}$ fulfills

$$\begin{cases} (\nabla\widetilde{w} \cdot \boldsymbol{t}_e)_{|e} = (\boldsymbol{\varphi} \cdot \boldsymbol{t}_e)_{|e} \in \mathbb{P}_0(e) & \text{on any } e \in \partial f,\\ \widetilde{w}_\tau \in H^1(f) & \text{in } f. \end{cases} \tag{4.4}$$

From (4.4) it follows that $\widetilde{w}$ restricted to the mesh skeleton is continuous and piecewise linear. Thus the function $\widetilde{w}$ is well defined (single valued) on the vertexes of the decomposition Ω_h and $\mathbf{D}_{\boldsymbol{V}}(\widetilde{w})$ makes sense. Let now $w \in W_h$ be the interpolant function of $\widetilde{w}$ in the sense of DoFs, i.e. the function uniquely determined by

$$\mathbf{D}_{\boldsymbol{V}}(w) = \mathbf{D}_{\boldsymbol{V}}(\widetilde{w}). \tag{4.5}$$

Inclusion ***(i1)*** guarantees that $\nabla w \in \boldsymbol{\Sigma}_h$. Hence, by Proposition 3.2, w realizes ***(i2)*** if and only if $\mathbf{D}_{\boldsymbol{\Sigma}}(\nabla w) = \mathbf{D}_{\boldsymbol{\Sigma}}(\boldsymbol{\varphi})$. Being $\mathbf{curl}(\nabla w) = \mathbf{curl}\,\boldsymbol{\varphi} = \mathbf{0}$, this reduce to verify that

$$\mathbf{D}^{\mathbf{5}}{}_{\boldsymbol{\Sigma}}(\nabla w) = \mathbf{D}^{\mathbf{5}}{}_{\boldsymbol{\Sigma}}(\boldsymbol{\varphi}).$$

For any edge e in the decomposition Ω_h, we denote with ν_2 and ν_1 the two endpoints of e, with $\boldsymbol{t}_e$ pointing from ν_1 to ν_2. Therefore, from (4.5) and (4.4), we infer

$$\begin{aligned}\mathbf{D^5}_{\boldsymbol{\Sigma},e}(\nabla w) &= \frac{1}{|e|}\int_e \nabla w\cdot\boldsymbol{t}_e\,\mathrm{d}s = \mathbf{D}_{\boldsymbol{V},\nu_2}(w)-\mathbf{D}_{\boldsymbol{V},\nu_1}(w) = \mathbf{D}_{\boldsymbol{V},\nu_2}(\widetilde{w})-\mathbf{D}_{\boldsymbol{V},\nu_1}(\widetilde{w})\\ &= \frac{1}{|e|}\int_e \nabla\widetilde{w}\cdot\boldsymbol{t}_e\,\mathrm{d}s = \frac{1}{|e|}\int_e \boldsymbol{\varphi}\cdot\boldsymbol{t}_e\,\mathrm{d}s = \mathbf{D^5}_{\boldsymbol{\Sigma},e}(\boldsymbol{\varphi}),\end{aligned}$$

that concludes the proof. □

Proposition 4.2. *Let* $\boldsymbol{\Sigma}_h$ *and* $\boldsymbol{Z}_h$ *be the spaces defined in* (3.28) *and* (3.12)*, respectively. Then*

$$\mathbf{curl}\,\boldsymbol{\Sigma}_h = \boldsymbol{Z}_h.$$

Proof. The proof follows by showing the following points:

(*i*1) for every $\boldsymbol{\varphi}\in\boldsymbol{\Sigma}_h$, $\mathbf{curl}\,\boldsymbol{\varphi}\in\boldsymbol{Z}_h$,
(*i*2) for every $\boldsymbol{v}\in\boldsymbol{Z}_h$, there exists $\boldsymbol{\varphi}\in\boldsymbol{\Sigma}_h$ such that $\mathbf{curl}\,\boldsymbol{\varphi}=\boldsymbol{v}$.

Let us analyze the inclusion **(*i*1)**. Let $\boldsymbol{\varphi}\in\boldsymbol{\Sigma}_h$, clearly $\mathbf{curl}\,\boldsymbol{\varphi}\in\boldsymbol{Z}(\Omega)$. Therefore, we need to verify that $(\mathbf{curl}\,\boldsymbol{\varphi})_{|P}\in\boldsymbol{V}_h(P)$ for any $P\in\Omega_h$. It is evident that the constraints in definition (3.17) are the **curl** version of the constraints in definition (3.7), and (ii) in (3.16) corresponds to (i) in (3.6). Hence it remains to show that $\mathbf{curl}\,\boldsymbol{\varphi}$ is the velocity solution of the Stokes problem associated with definition (3.7) on each element P.

By definition (3.17) the function $\boldsymbol{\varphi}$ satisfies

$$\int_P \boldsymbol{\Delta}\,\boldsymbol{\varphi}\cdot\boldsymbol{\Delta}\,\boldsymbol{\psi}\,\mathrm{d}P = \int_P \widetilde{\boldsymbol{p}}_{k-1}\cdot\boldsymbol{\psi}\,\mathrm{d}P,\quad \forall\,\boldsymbol{\psi}\in\boldsymbol{\Psi}_0(P),$$

which, recalling (3.20) and by an integration by parts, yields

$$\int_P \boldsymbol{\Delta}\,\boldsymbol{\varphi}\cdot\boldsymbol{\Delta}\,\boldsymbol{\psi}\,\mathrm{d}P = \int_P (\boldsymbol{x}\wedge\boldsymbol{p}_{k-1})\cdot\mathbf{curl}\,\boldsymbol{\psi}\,\mathrm{d}P,\quad \forall\,\boldsymbol{\psi}\in\boldsymbol{\Psi}_0(P). \tag{4.6}$$

In particular, the last equation is still valid restricting to all $\boldsymbol{\psi}\in\boldsymbol{\Psi}_0(P)\cap\boldsymbol{Z}(P)$. Therefore, using the identity $\boldsymbol{\Delta}=-\mathbf{curl}\,\mathbf{curl}+\boldsymbol{\nabla}\,\mathrm{div}$ and an integration by parts (coupled with the homogeneous boundary condition $\mathbf{curl}\,\boldsymbol{\psi}=0$ on ∂P), it is easy to show that (4.6) implies

$$\int_P -\boldsymbol{\Delta}(\mathbf{curl}\,\boldsymbol{\varphi})\cdot\mathbf{curl}\,\boldsymbol{\psi}\,\mathrm{d}P = \int_P (\boldsymbol{x}\wedge\boldsymbol{p}_{k-1})\cdot\mathbf{curl}\,\boldsymbol{\psi}\,\mathrm{d}P,\quad \forall\,\boldsymbol{\psi}\in\boldsymbol{\Psi}_0(P)\cap\boldsymbol{Z}(P). \tag{4.7}$$

Exploiting Lemma 5.1 in Ref. 43, for every $\boldsymbol{z} \in \boldsymbol{Z}_0(P)$ there exists $\boldsymbol{\psi} \in \boldsymbol{\Psi}_0(P) \cap \boldsymbol{Z}(P)$ such that $\boldsymbol{z} = \mathbf{curl}\,\boldsymbol{\psi}$. Therefore, (4.7) is equivalent to

$$\int_P \boldsymbol{\nabla}(\mathbf{curl}\,\boldsymbol{\varphi}) : \boldsymbol{\nabla}\boldsymbol{z}\,\mathrm{d}P = \int_P (\boldsymbol{x} \wedge \boldsymbol{p}_{k-1}) \cdot \boldsymbol{z}\,\mathrm{d}P \quad \text{for all } \boldsymbol{z} \in \boldsymbol{Z}_0(P),$$

and thus $\boldsymbol{v} = \mathbf{curl}\,\boldsymbol{\varphi}$ is the velocity solution of a Stokes problem as in definition (3.7). That concludes the proof for $\boldsymbol{(i1)}$.

We focus now on $\boldsymbol{(i2)}$. Let $\boldsymbol{v} \in \boldsymbol{Z}_h \subseteq \boldsymbol{Z}$, then from Corollary 3.3 in Ref. 43 there exists $\widetilde{\boldsymbol{\varphi}} \in [H^2(\Omega)]^3 \cap \boldsymbol{Z}(\Omega)$, such that $\mathbf{curl}\,\widetilde{\boldsymbol{\varphi}} = \boldsymbol{v}$. Notice that, being $\widetilde{\boldsymbol{\varphi}} \in [H^2(\Omega)]^3$ and $\mathbf{curl}\,\widetilde{\boldsymbol{\varphi}} \in \boldsymbol{V}_h(P)$ for any P in Ω_h, it makes sense to compute $\mathbf{D}_{\boldsymbol{\Sigma}}(\widetilde{\boldsymbol{\varphi}})$.

Let us consider the interpolant $\boldsymbol{\varphi} \in \boldsymbol{\Sigma}_h$ of $\widetilde{\boldsymbol{\varphi}}$ in the sense of DoFs, i.e. the function uniquely determined by (cf. Proposition 3.2)

$$\mathbf{D}_{\boldsymbol{\Sigma}}(\boldsymbol{\varphi}) = \mathbf{D}_{\boldsymbol{\Sigma}}(\widetilde{\boldsymbol{\varphi}}). \tag{4.8}$$

Property $\boldsymbol{(i1)}$ ensures $\mathbf{curl}\,\boldsymbol{\varphi} \in \boldsymbol{Z}_h$. Therefore, employing Proposition 3.1, $\boldsymbol{\varphi}$ realizes $\boldsymbol{(i2)}$ if and only if $\mathbf{D}_{\boldsymbol{V}}(\mathbf{curl}\,\boldsymbol{\varphi}) = \mathbf{D}_{\boldsymbol{V}}(\boldsymbol{v})$. Is it straightforward to check that

$$\mathbf{D^5}_{\boldsymbol{V}}(\mathbf{curl}\,\boldsymbol{\varphi}) = \mathbf{D^5}_{\boldsymbol{V}}(\boldsymbol{v}) = \mathbf{0},$$

$$\mathbf{D^i}_{\boldsymbol{V}}(\mathbf{curl}\,\boldsymbol{\varphi}) = \mathbf{D^i}_{\boldsymbol{\Sigma}}(\boldsymbol{\varphi}) = \mathbf{D^i}_{\boldsymbol{\Sigma}}(\widetilde{\boldsymbol{\varphi}}) = \mathbf{D^i}_{\boldsymbol{V}}(\boldsymbol{v}) \quad \text{for } \boldsymbol{i} = \mathbf{1,2,3,4},$$

except for the face moment (that is slightly more subtle)

$$\int_f \mathbf{curl}\,\boldsymbol{\varphi} \cdot \boldsymbol{n}_P^f\,\mathrm{d}f \quad \text{and} \quad \int_f \boldsymbol{v} \cdot \boldsymbol{n}_P^f\,\mathrm{d}f \quad \text{for any face } f.$$

In order to show that the two quantities above are equal we exploit the same computations in (3.24) and (4.8)

$$\begin{aligned}\int_f \mathbf{curl}\,\boldsymbol{\varphi} \cdot \boldsymbol{n}_P^f\,\mathrm{d}f &= \sum_{e \in \partial f} |e|\,\mathbf{D^5}_{\boldsymbol{\Sigma},e}(\boldsymbol{\varphi})\,\boldsymbol{t}_e \cdot \boldsymbol{t}_f^e = \sum_{e \in \partial f} |e|\,\mathbf{D^5}_{\boldsymbol{\Sigma},e}(\widetilde{\boldsymbol{\varphi}})\,\boldsymbol{t}_e \cdot \boldsymbol{t}_f^e \\ &= \int_f \mathbf{curl}\,\widetilde{\boldsymbol{\varphi}} \cdot \boldsymbol{n}_P^f\,\mathrm{d}f = \int_f \boldsymbol{v} \cdot \boldsymbol{n}_P^f\,\mathrm{d}f.\end{aligned}$$

This ends the proof. □

Proposition 4.3. *Let $\boldsymbol{V}_h$ and Q_h be the spaces defined in* (3.10) *and* (3.3)*, respectively. Then*

$$\operatorname{div} \boldsymbol{V}_h = Q_h.$$

Proof. We follow same strategy adopted in the previous propositions and show that

- $\boldsymbol{(i1)}$ for every $\boldsymbol{v} \in \boldsymbol{V}_h$, $\operatorname{div} \boldsymbol{v} \in Q_h$,
- $\boldsymbol{(i2)}$ for every $q \in Q_h$ there exists $\boldsymbol{v} \in \boldsymbol{V}_h$ such that $\operatorname{div} \boldsymbol{v} = q$.

The inclusion **(*i*1)** is trivial. Regarding the point **(*i*2)**, since (2.7) is an exact sequence, for any $q \in Q_h$ there exists $\widetilde{\boldsymbol{v}} \in [H^1(\Omega)]^3$ such that $\operatorname{div} \widetilde{\boldsymbol{v}} = q$. Now let $\boldsymbol{v} \in \boldsymbol{V}_h$ the function uniquely determined by (cf. Proposition 3.1)

$$\mathbf{D^1}_{\boldsymbol{V}}(\boldsymbol{v}) = \mathbf{D^2}_{\boldsymbol{V}}(\boldsymbol{v}) = \mathbf{D^4}_{\boldsymbol{V}}(\boldsymbol{v}) = \mathbf{0},$$

$$\mathbf{D^3}_{\boldsymbol{V}}(\boldsymbol{v}) = \mathbf{0} \quad \text{except the face moments } \int_f \boldsymbol{v} \cdot \boldsymbol{n}_P^f \,\mathrm{d}f = \int_f \widetilde{\boldsymbol{v}} \cdot \boldsymbol{n}_P^f \,\mathrm{d}f, \tag{4.9}$$

$$\mathbf{D^5}_{\boldsymbol{V}}(\boldsymbol{v}) = \mathbf{D^5}_{\boldsymbol{V}}(\widetilde{\boldsymbol{v}}).$$

Notice that being $\widetilde{\boldsymbol{v}} \in [H^1(\Omega)]^3$ the face moments in (4.9) and $\mathbf{D^5}_{\boldsymbol{V}}(\widetilde{\boldsymbol{v}})$ are actually well defined. Therefore, for any $P \in \Omega_h$ we infer

$$\int_P (\operatorname{div} \boldsymbol{v}) \widehat{\boldsymbol{p}}_{k-1} \,\mathrm{d}P = \int_P (\operatorname{div} \widetilde{\boldsymbol{v}}) \widehat{\boldsymbol{p}}_{k-1} \,\mathrm{d}P = \int_P q \, \widehat{\boldsymbol{p}}_{k-1} \,\mathrm{d}P \quad \text{for all } \widehat{\boldsymbol{p}}_{k-1} \in \widehat{\mathbb{P}}_{k-1\backslash 0}(P). \tag{4.10}$$

Moreover, employing the divergence theorem, (4.9) implies

$$\begin{aligned} \int_P \operatorname{div} \boldsymbol{v} \,\mathrm{d}P &= \int_{\partial P} \boldsymbol{v} \cdot \boldsymbol{n}_P \,\mathrm{d}f = \sum_{f \in \partial P} \int_f \boldsymbol{v} \cdot \boldsymbol{n}_P^f \,\mathrm{d}f \\ &= \sum_{f \in \partial P} \int_f \widetilde{\boldsymbol{v}} \cdot \boldsymbol{n}_P^f \,\mathrm{d}f = \int_{\partial P} \widetilde{\boldsymbol{v}} \cdot \boldsymbol{n}_P \,\mathrm{d}f = \int_P \operatorname{div} \widetilde{\boldsymbol{v}} \,\mathrm{d}P = \int_P q \,\mathrm{d}P. \end{aligned} \tag{4.11}$$

Notice that (4.10) and (4.11) coincide with $\mathbf{D}_Q(\operatorname{div} \boldsymbol{v}) = \mathbf{D}_Q(q)$ that coupled with $\operatorname{div} \boldsymbol{v} \in Q_h$ (from **(*i*1)**) concludes the proof. □

5. Virtual Elements for the 3D Navier–Stokes Equation

We consider the steady Navier–Stokes equation on a polyhedral domain $\Omega \subseteq \mathbb{R}^3$ with homogeneous Dirichlet boundary conditions:

$$\begin{cases} \text{find } (\boldsymbol{u},\, p) \in [H_0^1(\Omega)]^3 \times L_0^2(\Omega), & \text{such that} \\ \nu a(\boldsymbol{u}, \boldsymbol{v}) + c(\boldsymbol{u}; \boldsymbol{u}, \boldsymbol{v}) + b(\boldsymbol{v}, p) = (\boldsymbol{f}, \boldsymbol{v}) & \text{for all } \boldsymbol{v} \in [H_0^1(\Omega)]^3, \\ b(\boldsymbol{u}, q) = 0 & \text{for all } q \in Q, \end{cases} \tag{5.1}$$

where $\nu > 0$ represents the viscosity, $\boldsymbol{f} \in [L^2(\Omega)]^3$ is the external force and

$$a(\boldsymbol{u}, \boldsymbol{v}) := \int_\Omega \boldsymbol{\varepsilon}(\boldsymbol{u}) : \boldsymbol{\varepsilon}(\boldsymbol{v}) \mathrm{d}\Omega \quad \text{for all } \boldsymbol{u},\, \boldsymbol{v} \in [H^1(\Omega)]^3, \tag{5.2}$$

$$c(\boldsymbol{w}; \boldsymbol{u}, \boldsymbol{v}) := \int_\Omega [(\boldsymbol{\nabla}\, \boldsymbol{u})\boldsymbol{w}] \cdot \boldsymbol{v} \,\mathrm{d}\Omega \quad \text{for all } \boldsymbol{w},\, \boldsymbol{u},\, \boldsymbol{v} \in [H^1(\Omega)]^3, \tag{5.3}$$

$$b(\boldsymbol{u}, q) := \int_\Omega \operatorname{div} \boldsymbol{u}\, q \,\mathrm{d}\Omega \quad \text{for all } \boldsymbol{u} \in [H^1(\Omega)]^3 \text{ and } q \in L^2(\Omega). \tag{5.4}$$

For sake of simplicity we here consider Dirichlet homogeneous boundary conditions, different boundary conditions can be treated as well.

It is well known[54] that in the diffusion dominated regime

$$(\mathbf{H}) \quad \gamma := \frac{\|\boldsymbol{f}\|_{-1}}{\nu^2} \ll 1$$

the Navier–Stokes equation (5.1) has a unique solution $(\boldsymbol{u}, p)$ with

$$|\boldsymbol{u}|_1 \leq \frac{\|\boldsymbol{f}\|_{-1}}{\nu}.$$

A sharper estimate on γ and $|\boldsymbol{u}|_1$ can be obtained employing the Helmholtz–Hodge projection of the load f (we refer the reader to Ref. 46 and the references therein). Moreover, problem (5.1) can be formulated in the equivalent kernel form:

$$\begin{cases} \text{find } \boldsymbol{u} \in \boldsymbol{Z}_0(\Omega), & \text{such that} \\ \nu a(\boldsymbol{u}, \boldsymbol{v}) + c(\boldsymbol{u}; \boldsymbol{u}, \boldsymbol{v}) = (\boldsymbol{f}, \boldsymbol{v}) & \text{for all } \boldsymbol{v} \in \boldsymbol{Z}_0(\Omega). \end{cases}$$

5.1. *Discrete forms and load term approximation*

In this subsection, we briefly describe the construction of a discrete version of the bilinear form $a(\cdot, \cdot)$ given in (5.2) and trilinear form $c(\cdot; \cdot, \cdot)$ given in (5.3). We can follow in a rather slavish way the procedure initially introduced in Ref. 10 for the Laplace problem and further developed in Ref. 18 for flow problems. First, we decompose into local contributions the bilinear form $a(\cdot, \cdot)$ and the trilinear form $c(\cdot; \cdot, \cdot)$ by considering

$$a(\boldsymbol{u}, \boldsymbol{v}) =: \sum_{P \in \Omega_h} a^P(\boldsymbol{u}, \boldsymbol{v}), \quad c(\boldsymbol{w}; \boldsymbol{u}, \boldsymbol{v}) =: \sum_{P \in \Omega_h} c^P(\boldsymbol{w}; \boldsymbol{u}, \boldsymbol{v}),$$

for all $\boldsymbol{w}$, $\boldsymbol{u}$, $\boldsymbol{v} \in [H^1(\Omega)]^3$.

As usual in VEM framework the discrete counterpart of the continuous forms above is defined starting from the polynomial projections defined in (3.1) and (3.2). The following proposition extends to the 3D case the result for the bi-dimensional spaces.[17,57]

Proposition 5.1. *Let $\widehat{\mathbb{B}}_k(f)$ and $\boldsymbol{V}_h(P)$ be the spaces defined in* (3.5) *and* (3.7)*, respectively. The DoFs $\mathbf{D}_{\boldsymbol{V}}$ allow us to compute exactly the face projections*

$$\Pi_k^{\nabla,f} : [\widehat{\mathbb{B}}_k(f)]^3 \to [\mathbb{P}_k(f)]^3, \quad \Pi_{k+1}^{0,f} : [\widehat{\mathbb{B}}_k(f)]^3 \to [\mathbb{P}_{k+1}(f)]^3,$$

for any $f \in \partial P$, and the element projections

$$\Pi_k^{\nabla,P} : \boldsymbol{V}_h(P) \to [\mathbb{P}_k(P)]^3,$$

$$\boldsymbol{\Pi}_{k-1}^{0,P} : \boldsymbol{\nabla}(\boldsymbol{V}_h(P)) \to [\mathbb{P}_{k-1}(P)]^{3\times 3},$$

$$\Pi_k^{0,P} : \boldsymbol{V}_h(P) \to [\mathbb{P}_k(P)]^3,$$

in the sense that, given any $\boldsymbol{v}_h \in \boldsymbol{V}_h(P)$*, we are able to compute the polynomials*

$$\Pi_k^{\nabla,f}\boldsymbol{v}_h, \quad \Pi_{k+1}^{0,f}\boldsymbol{v}_h, \quad \Pi_k^{\nabla,P}\boldsymbol{v}_h, \quad \boldsymbol{\Pi}_k^{0,P}(\boldsymbol{\nabla}\boldsymbol{v}_h), \quad \Pi_k^{0,P}\boldsymbol{v}_h,$$

using only, as unique information, the DoFs values $\mathbf{D}_{\boldsymbol{V}}$ *of* $\boldsymbol{v}_h$*.*

Proof. The computability of the face projections is a direct application of Remark 5 in Ref. 2. Concerning the element projections we here limit to prove the last item, the first two follow analogous techniques.

By definition of L^2-projection (3.1), in order to determine, for any $\boldsymbol{v} \in \boldsymbol{V}_h(P)$, the polynomial $\Pi_k^{0,P}\boldsymbol{v}$ we need to compute

$$\int_P \boldsymbol{v}\cdot\boldsymbol{p}_k \,\mathrm{d}P \quad \text{for all } \boldsymbol{p}_k \in [\mathbb{P}_k(P)]^3.$$

From polynomial decomposition (2.2) we can write

$$\boldsymbol{p}_k = \nabla\widehat{p}_{k+1} + \boldsymbol{x}\wedge\widehat{\boldsymbol{q}}_{k-1} + \boldsymbol{x}\wedge\boldsymbol{q}_{k-3}$$

for some $\widehat{p}_{k+1} \in \widehat{\mathbb{P}}_{k+1\backslash 0}(P)$, $\widehat{\boldsymbol{q}}_{k-1} \in [\widehat{\mathbb{P}}_{k-1\backslash k-3}(P)]^3$, $\boldsymbol{q}_{k-3} \in [\mathbb{P}_{k-3}(P)]^3$. Thus

$$\begin{aligned}
\int_P \boldsymbol{v}\cdot\boldsymbol{p}_k \,\mathrm{d}P &= \int_P \boldsymbol{v}\cdot(\nabla\widehat{p}_{k+1} + \boldsymbol{x}\wedge\widehat{\boldsymbol{q}}_{k-1} + \boldsymbol{x}\wedge\boldsymbol{q}_{k-3})\mathrm{d}P \\
&= \int_P \Pi_k^{\nabla,P}\boldsymbol{v}\cdot(\boldsymbol{x}\wedge\widehat{\boldsymbol{q}}_{k-1})\mathrm{d}P + \int_P \boldsymbol{v}\cdot(\boldsymbol{x}\wedge\boldsymbol{q}_{k-3})\mathrm{d}P \\
&\qquad\qquad \text{(enhancing def. (3.7))} \\
&\quad - \int_P (\operatorname{div}\boldsymbol{v})\widehat{p}_{k+1}\,\mathrm{d}P + \int_{\partial P}\boldsymbol{v}\cdot\boldsymbol{n}_P\widehat{p}_{k+1}\,\mathrm{d}f \qquad \text{(integration by parts)} \\
&= \int_P \Pi_k^{\nabla,P}\boldsymbol{v}\cdot(\boldsymbol{x}\wedge\widehat{\boldsymbol{q}}_{k-1})\mathrm{d}P + \int_P \boldsymbol{v}\cdot(\boldsymbol{x}\wedge\boldsymbol{q}_{k-3})\mathrm{d}P \\
&\quad - \int_P (\operatorname{div}\boldsymbol{v})\widehat{p}_{k+1}\,\mathrm{d}P + \sum_{f\in\partial P}\int_f (\Pi_{k+1}^{0,f}\boldsymbol{v})\cdot\boldsymbol{n}_P^f\widehat{p}_{k+1}\,\mathrm{d}f \quad \text{(by def. (3.1))}.
\end{aligned}$$

The first and the last integrals are computable being $\Pi_k^{\nabla,P}\boldsymbol{v}$ and $\Pi_{k+1}^{0,f}$ computable. The second addend corresponds to the DoFs $\mathbf{D}^{\mathbf{4}}{}_{\boldsymbol{V}}$. For the third addend we observe that, since $\operatorname{div}\boldsymbol{v}$ is a polynomial of degree less than or equal to $k-1$ we can exactly reconstruct its value from the DoFs $\mathbf{D}^{\mathbf{5}}{}_{\boldsymbol{V}}$ and the normal face moments in $\mathbf{D}^{\mathbf{3}}{}_{\boldsymbol{V}}$. □

On the basis of the projections above, following a standard procedure in the VEM framework, we define the computable (in the sense of Proposition 5.1) discrete local forms and the approximated right-hand side

$$a_h^P(\boldsymbol{u},\boldsymbol{v}) := \int_P (\boldsymbol{\Pi}_{k-1}^{0,P}\boldsymbol{\varepsilon}(\boldsymbol{u})) : (\boldsymbol{\Pi}_{k-1}^{0,P}\boldsymbol{\varepsilon}(\boldsymbol{v}))\mathrm{d}P + \mathcal{S}^P((I-\Pi_k^{\nabla,P})\boldsymbol{u},\,(I-\Pi_k^{\nabla,P})\boldsymbol{v}), \tag{5.5}$$

$$c_h^P(\boldsymbol{w};\boldsymbol{u},\boldsymbol{v}) := \int_P [(\boldsymbol{\Pi}_{k-1}^{0,P}\boldsymbol{\nabla}\boldsymbol{u})\boldsymbol{\Pi}_k^{0,P}\boldsymbol{w}]\cdot\boldsymbol{\Pi}_k^{0,P}\boldsymbol{v}\,\mathrm{d}P, \tag{5.6}$$

$$(\boldsymbol{f}_h,\boldsymbol{v})_P := \int_P \boldsymbol{\Pi}_k^{0,P}\boldsymbol{f}\cdot\boldsymbol{v}\,\mathrm{d}P, \tag{5.7}$$

for all $\boldsymbol{w}$, $\boldsymbol{u}$, $\boldsymbol{v}\in\boldsymbol{V}_h(P)$, where clearly

$$\boldsymbol{\Pi}_{k-1}^{0,P}\boldsymbol{\varepsilon}(\boldsymbol{v}) = \frac{\boldsymbol{\Pi}_{k-1}^{0,P}\boldsymbol{\nabla}\boldsymbol{v} + (\boldsymbol{\Pi}_{k-1}^{0,P}\boldsymbol{\nabla}\boldsymbol{v})^{\mathrm{T}}}{2}$$

and the symmetric stabilizing form $\mathcal{S}^P\colon \boldsymbol{V}_h(P)\times\boldsymbol{V}_h(P)\to\mathbb{R}$ satisfies

$$|\boldsymbol{v}|_{1,P}^2 \lesssim \mathcal{S}^P(\boldsymbol{v},\boldsymbol{v}) \lesssim |\boldsymbol{v}|_{1,P}^2 \quad \text{for all } \boldsymbol{v}\in\mathrm{Ker}(\Pi_k^{\nabla,P}).$$

The condition above essentially requires the stabilizing term $\mathcal{S}^P(\boldsymbol{v},\boldsymbol{v})$ to scale as $|\boldsymbol{v}|_{1,P}^2$. For instance, a standard choice for the stabilization is the D-recipe stabilization introduced in Ref. 15.

Remark 5.1. The H^1-seminorm projection $\Pi_k^{\nabla,P}$ in the stabilization term of definition (5.5) can be replaced by any polynomial projection Π_k^P that is computable on the basis of the DoFs $\mathbf{D}_{\boldsymbol{V}}$ (in the sense of Proposition 5.1). A possible choice will be explored in Sec. 6.

The global virtual forms and the global approximated right-hand side are defined by simply summing the local contributions:

$$\begin{aligned} a_h(\boldsymbol{u},\boldsymbol{v}) &:= \sum_{P\in\Omega_h} a_h^P(\boldsymbol{u},\boldsymbol{v}),\\ c_h(\boldsymbol{w};\boldsymbol{u},\boldsymbol{v}) &:= \sum_{P\in\Omega_h} c_h^P(\boldsymbol{w};\boldsymbol{u},\boldsymbol{v}),\\ (\boldsymbol{f}_h,\boldsymbol{v}) &:= \sum_{P\in\Omega_h} (\boldsymbol{f}_h,\boldsymbol{v})_P, \end{aligned} \tag{5.8}$$

for all $\boldsymbol{w}$, $\boldsymbol{u}$, $\boldsymbol{v}\in\boldsymbol{V}_h$.

5.2. *The discrete problem*

Referring to the discrete spaces (3.10), (3.3), the discrete forms and the approximated load term (5.8) and the div form (5.4), the virtual element approximation of the Navier–Stokes equation is given by

$$\begin{cases} \text{find } (\boldsymbol{u}_h,p_h)\in\boldsymbol{V}_{h,0}\times Q_{h,0}, & \text{such that}\\ \nu a_h(\boldsymbol{u}_h,\boldsymbol{v}_h) + c_h(\boldsymbol{u}_h;\boldsymbol{u}_h,\boldsymbol{v}_h) + b(\boldsymbol{v}_h,p_h) = (\boldsymbol{f}_h,\boldsymbol{v}_h) & \text{for all } \boldsymbol{v}_h\in\boldsymbol{V}_{h,0},\\ b(\boldsymbol{u}_h,q_h) = 0 & \text{for all } q_h\in Q_{h,0}, \end{cases} \tag{5.9}$$

where $\boldsymbol{V}_{h,0} := \boldsymbol{V}_h\cap[H_0^1(\Omega)]^3$ and $Q_{h,0} := Q_h\cap L_0^2(\Omega)$.

Recalling the kernel inclusion (3.13), problem (5.9) can be also formulated in the equivalent kernel form

$$\begin{cases} \text{find } \boldsymbol{u}_h \in \boldsymbol{Z}_{h,0}, & \text{such that} \\ \nu a_h(\boldsymbol{u}_h, \boldsymbol{v}_h) + c_h(\boldsymbol{u}_h; \boldsymbol{u}_h, \boldsymbol{v}_h) = (\boldsymbol{f}_h, \boldsymbol{v}_h) & \text{for all } \boldsymbol{v}_h \in \boldsymbol{Z}_{h,0}, \end{cases} \tag{5.10}$$

with the obvious notation $\boldsymbol{Z}_{h,0} := \boldsymbol{Z}_h \cap [H^1_0(\Omega)]^3$.

Combining the arguments in Refs. 17, 18, 26 it is possible to show that the virtual space $\boldsymbol{V}_h$ has an optimal interpolation order of accuracy with respect to the degree k, and that the couple of spaces $(\boldsymbol{V}_h, Q_h)$ is inf-sup stable.[23] The following existence and convergence theorem extends the analogous result for the bi-dimensional case.[18]

Theorem 5.1. *Under the assumptions* (**A1**)–(**A3**) *and* (**H**), *let* $(\boldsymbol{u}, p) \in [H^1_0(\Omega)]^3 \times L^2_0(\Omega)$ *be the solution of problem* (5.1) *and* $(\boldsymbol{u}_h, p_h) \in \boldsymbol{V}_{h,0} \times Q_{h,0}$ *be the* (*unique*) *solution of problem* (5.9). *Assuming moreover* $\boldsymbol{u}, \boldsymbol{f} \in [H^{s+1}(\Omega)]^3$ *and* $p \in H^s(\Omega)$, $0 < s \leq k$, *then*

$$|\boldsymbol{u} - \boldsymbol{u}_h|_1 \lesssim h^s \mathcal{F}(\boldsymbol{u}; \nu, \gamma) + h^{s+2} \mathcal{H}(\boldsymbol{f}; \nu), \tag{5.11}$$

$$\|p - p_h\|_0 \lesssim h^s |p|_s + h^s \mathcal{K}(\boldsymbol{u}; \nu, \gamma) + h^{s+2} |\boldsymbol{f}|_{s+1} \tag{5.12}$$

for suitable functions $\mathcal{F}$, $\mathcal{H}$, $\mathcal{K}$ *independent of* h.

Note that, as a consequence of the important property (3.13), there is no direct dependence of the velocity error on the pressure solution.

Remark 5.2. Since Proposition 4.2 yields an explicit characterization of $\boldsymbol{Z}_h$ as $\mathbf{curl}\, \boldsymbol{\Sigma}_h$, one could follow (5.10) and build an equivalent **curl** (discrete) formulation (see for instance problem (77) in Ref. 19). Such approach is less appealing in 3D since the **curl** operator has a nontrivial kernel and thus some stabilization or additional Lagrange multiplier would be needed in the formulation. Moreover, this approach does not seem to be competitive in terms of number of DoFs with the reduced version of the method (see Sec. 5.3). As a consequence, we do not explore any scheme resulting from the **curl** formulation.

5.3. *Reduced spaces and reduced scheme*

In this section, we briefly show that problem (5.9) is somehow equivalent to a suitable reduced problem entangling relevant fewer DoFs, especially for large k. This reduction is analogous to its 2D counterpart in Sec. 5 in Ref. 17 and Sec. 5.2 in Ref. 57.

The core idea is that $\mathbf{D^5_V}(\boldsymbol{u}_h) = \mathbf{0}$, where $\boldsymbol{u}_h$ denotes the solution of (5.9), and therefore such DoFs (and also the associated pressures) can be trivially eliminated from the system. Hence on each polygon P, let us define the reduced local spaces:

$$\widehat{\boldsymbol{V}}_h(P) := \{\boldsymbol{v} \in [H^1(P)]^3 \text{ s.t. (i) } \boldsymbol{v}_{|\partial P} \in [\widehat{\mathbb{B}}_k(\partial P)]^3$$
$$\text{(ii) } \boldsymbol{\Delta v} + \nabla s \in \boldsymbol{x} \wedge [\mathbb{P}_{k-1}(P)]^3 \text{ for some } s \in L^2_0(P)$$

(iii) $\operatorname{div} \boldsymbol{v} \in \mathbb{P}_0(P)$,

(iv) $(\boldsymbol{v} - \Pi_k^{\nabla,P}\boldsymbol{v}, \boldsymbol{x}\wedge\widehat{\boldsymbol{p}}_{k-1})_P = 0,\ \forall\, \widehat{\boldsymbol{p}}_{k-1} \in [\widehat{\mathbb{P}}_{k-1\setminus k-3}(P)]^3\}$

and

$$\widehat{Q}_h(P) := \mathbb{P}_0(P).$$

Exploiting the same tools of Proposition 3.1 it can be proved that the linear operators $\widehat{\mathbf{D}}_{\boldsymbol{V}}$ split into four subsets, defined by

$$\widehat{\mathbf{D}}^{\boldsymbol{i}}_{\boldsymbol{V}} = \mathbf{D}^{\boldsymbol{i}}{}_{\boldsymbol{V}} \quad \text{for } \boldsymbol{i} = \mathbf{1,2,3,4},$$

constitute a set of DoFs for $\widehat{\boldsymbol{V}}_h(P)$. Concerning the space $\widehat{Q}_h(P)$, it is straightforward to see that $\dim(\widehat{Q}_h(P)) = 1$ with unique DoF $\widehat{\mathbf{D}}_Q$ defined by $\widehat{\mathbf{D}}_Q(q) := \int_P q\,\mathrm{d}P$. The global spaces $\widehat{\boldsymbol{V}}_h$ and $\widehat{Q}_h$ are obtained in the standard fashion by gluing the local spaces:

$$\widehat{\boldsymbol{V}}_h := \{\boldsymbol{v} \in [H^1(\Omega)]^3 \text{ s.t. } \boldsymbol{v}_{|P} \in \widehat{\boldsymbol{V}}_h(P) \text{ for all } P \in \Omega_h\}, \tag{5.13}$$

$$\widehat{Q}_h := \{q \in L^2(\Omega) \text{ s.t. } q_{|P} \in \widehat{Q}_h(P) \text{ for all } P \in \Omega_h\}. \tag{5.14}$$

We remark that by construction $\boldsymbol{Z}_h \subseteq \widehat{\boldsymbol{V}}_h$, therefore employing Propositions 4.1 and 4.2 we can state the following result.

Proposition 5.2. *Referring to* (3.31), (3.28), (5.13) *and* (5.14), *the sequence*

$$\mathbb{R} \xrightarrow{\ i\ } W_h \xrightarrow{\ \nabla\ } \boldsymbol{\Sigma}_h \xrightarrow{\ \mathbf{curl}\ } \widehat{\boldsymbol{V}}_h \xrightarrow{\ \operatorname{div}\ } \widehat{Q}_h \xrightarrow{\ 0\ } 0$$

is an exact sub-complex of (2.7).

Referring to (5.13), (5.14) and (5.8), we consider the reduced problem:

$$\begin{cases} \text{find } (\widehat{\boldsymbol{u}}_h, \widehat{p}_h) \in \widehat{\boldsymbol{V}}_{h,0} \times \widehat{Q}_{h,0}, & \text{such that} \\ \nu a_h(\widehat{\boldsymbol{u}}_h, \boldsymbol{v}_h) + c_h(\widehat{\boldsymbol{u}}_h; \widehat{\boldsymbol{u}}_h, \boldsymbol{v}_h) + b(\boldsymbol{v}_h, \widehat{p}_h) = (\boldsymbol{f}_h, \boldsymbol{v}_h) & \text{for all } \boldsymbol{v}_h \in \widehat{\boldsymbol{V}}_{h,0}, \\ b(\widehat{\boldsymbol{u}}_h, q_h) = 0 & \text{for all } q_h \in \widehat{Q}_{h,0}, \end{cases} \tag{5.15}$$

where $\widehat{\boldsymbol{V}}_{h,0} := \widehat{\boldsymbol{V}}_h \cap [H^1_0(\Omega)]^3$ and $\widehat{Q}_{h,0} := \widehat{Q}_h \cap L^2_0(\Omega)$.

It is trivial to check that the reduced scheme (5.15) has $(2\pi_{k-1,3} - 2)N_P$ DoFs less when compared with the original one (5.9).

The following proposition is easy to check and states the relation between problem (5.9) and the reduced problem (5.15).

Proposition 5.3. *Let* $(\boldsymbol{u}_h, p_h) \in \boldsymbol{V}_h \times Q_h$ *and* $(\widehat{\boldsymbol{u}}_h, \widehat{p}_h) \in \widehat{\boldsymbol{V}}_h \times \widehat{Q}_h$ *be the solution of problem* (5.9) *and problem* (5.15), *respectively. Then*

$$\widehat{\boldsymbol{u}}_h = \boldsymbol{u}_h \quad \textit{and} \quad \widehat{p}_h = \Pi_0^{0,P} p_h \quad \textit{in every } P \in \Omega_h.$$

6. Numerical Validation

In this section, we numerically verify the proposed discretization scheme. Before dealing with such examples, we briefly describe an alternative (computationally cheaper) projection adopted in the implementation of the method. Then we outline the polyhedral meshes and the error norms used in the analysis.

6.1. *An alternative DoF-based projection*

In the light of Remarks 3.1 and 5.1, the aim of this subsection is to exhibit an alternative projection to be used in the place of the standard H^1-seminorm projection $\Pi_k^{\nabla,P}$ in (3.7) and (5.5) that will turn out to be very easy to implement. An analogous alternative projection could also be used to substitute $\Pi_k^{\nabla,f}$ in (3.5).

For any element $P \in \Omega_h$, let $\mathtt{NDoF} := \dim(\boldsymbol{V}_h(P))$. Then referring to Proposition 3.1 we set $\mathbf{D}_{\boldsymbol{V}} := \{\mathbf{D}_{\boldsymbol{V},i}\}_{i=1}^{\mathtt{NDoF}}$, and we denote with $\mathcal{D}\colon \boldsymbol{V}_h(P) \to \mathbb{R}^{\mathtt{NDoF}}$ the linear operator defined for all $\boldsymbol{v} \in \boldsymbol{V}_h(P)$ by

$$(\mathcal{D}\,\boldsymbol{v})_i = \mathbf{D}_{\boldsymbol{V},i}(\boldsymbol{v}) \quad \text{for } i = 1, \dots, \mathtt{NDoF},$$

i.e. $\mathcal{D}\,\boldsymbol{v}$ is the vector containing the DoF values $\mathbf{D}_{\boldsymbol{V}}$ associated to $\boldsymbol{v}$. We consider:

- the *DoF-projection* $\Pi_n^{\mathcal{D},P}\colon \boldsymbol{V}_h(P) \to [\mathbb{P}_n(P)]^3$ defined for any $\boldsymbol{v} \in \boldsymbol{V}_h(P)$ by

$$(\mathcal{D}\,\boldsymbol{q}_n, \mathcal{D}(\boldsymbol{v} - \Pi_n^{\mathcal{D},P}\boldsymbol{v}))_{\mathbb{R}^{\mathtt{NDoF}}} = 0 \quad \text{for all } \boldsymbol{q}_n \in [\mathbb{P}_n(P)]^3. \tag{6.1}$$

Notice that $\Pi_n^{\mathcal{D},P}$ is a special case of the serendipity projection introduced in Ref. 14.

Although the projection $\Pi_n^{\mathcal{D},P}$ may seem awkward on paper, it is quite simple and cheap to implement on the computer (since it is nothing but an Euclidean projection with respect to the DoF vectors). Indeed, it can be checked that the matrix formulation $\mathbf{\Pi}_n^{\mathcal{D},P}$ of the operator $\Pi_n^{\mathcal{D},P}$ acting from $\boldsymbol{V}_h(P)$ to $\boldsymbol{V}_h(P)$ (containing $[\mathbb{P}_n(P)]^3$) with respect to the basis $\boldsymbol{\mathcal{V}}$ (cf. Ref. 12, formula (3.18)) is

$$\mathbf{\Pi}_n^{\mathcal{D},P} = D(D^T D)^{-1} D^T \in \mathbb{R}^{\mathtt{NDoF}\times\mathtt{NDoF}},$$

where $D \in \mathbb{R}^{\mathtt{NDoF}\times 3\pi_{n,3}}$ is the matrix defined by (cf. Ref. 12, formula (3.17))

$$D_{i,\alpha} := \mathbf{D}_{\boldsymbol{V},i}(\boldsymbol{m}_\alpha) \quad \text{for } i = 1, \dots, \mathtt{NDoF} \text{ and } \alpha = 1, \dots, 3\pi_{n,3},$$

where using standard VEM notation, $\boldsymbol{m}_\alpha$ denotes the scaled monomial

$$\boldsymbol{m}_\alpha := \left(\left(\frac{\boldsymbol{x} - \boldsymbol{x}_B}{h_P}\right)^{\boldsymbol{\alpha_1}}, \left(\frac{\boldsymbol{x} - \boldsymbol{x}_B}{h_P}\right)^{\boldsymbol{\alpha_2}}, \left(\frac{\boldsymbol{x} - \boldsymbol{x}_B}{h_P}\right)^{\boldsymbol{\alpha_3}}\right)^T$$

with $\boldsymbol{x}_B$ barycenter of the polyhedron P, and $\boldsymbol{\alpha_1}$, $\boldsymbol{\alpha_2}$ and $\boldsymbol{\alpha_3}$ suitable multi-indexes.

6.2. *Meshes and error norms*

We consider the standard $[0, 1]^3$ cube as domain Ω and we make four different discretizations of such domain:

(1) *Structured* refers to meshes composed by structured cubes inside the domain, Fig. 1(a).

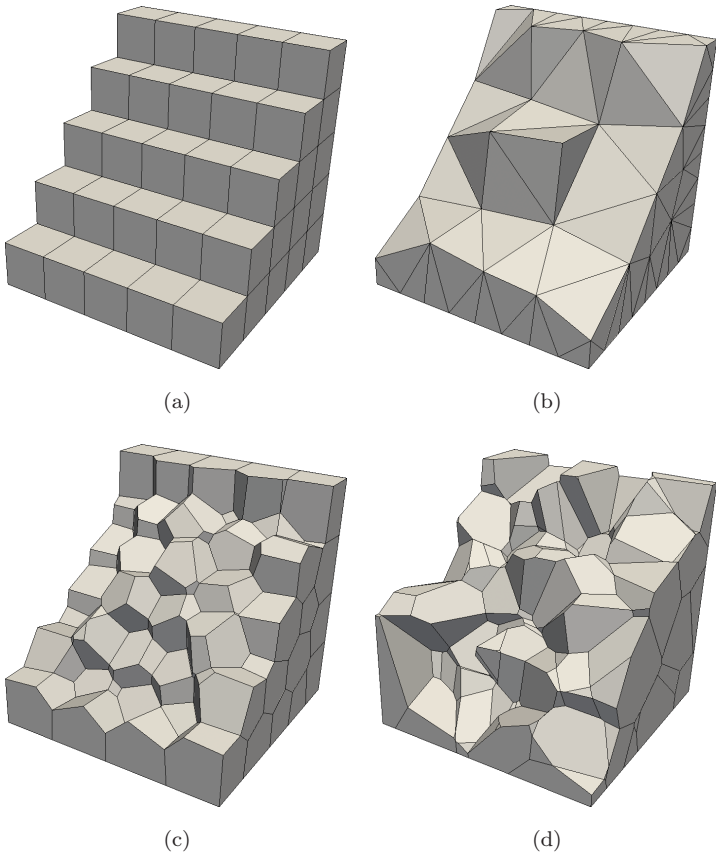

Fig. 1. Adopted mesh types: (a) structured, (b) tetra, (c) CVT and (d) random.

(2) *Tetra* is a constrained Delaunay tetrahedralization of Ω, Fig. 1(b).
(3) *CVT* refers to a Centroidal Voronoi Tessellation, i.e. a Voronoi tessellation where the control points coincide with the centroid of the cells they define, Fig. 1(c).
(4) *Random* is a Voronoi diagram of a point set randomly displayed inside the domain Ω, Fig. 1(d).

We would like to underline that the last type of mesh will severely test the robustness of the proposed method. Indeed, *Random* meshes are characterized by elements whose faces can be very small and distorted, see the details in Fig. 1(d).

The tetrahedral meshes are generated via `tetgen`,[56] while the last two are obtained by exploiting the c++ library `voro++`.[55] To analyze the error convergence rate, we make, for each family, a sequence of four meshes with decreasing size. For each mesh we define the mesh-size as

$$h := \frac{1}{L_P} \sum_{P \in \Omega_h} h_P.$$

Let $(\boldsymbol{u}, p)$ and $(\boldsymbol{u}_h, p_h)$ be the continuous and discrete VEM solution of the Stokes (or Navier–Stokes problem) under study. To evaluate how this discrete solution is close to the exact one, we use the following error measures, that make use of the local projection described in Proposition 5.1:

- H^1*-velocity error*:

$$e^{\boldsymbol{u}}_{H^1} := \sqrt{\sum_{P\in\Omega_h} ||\nabla \boldsymbol{u} - \boldsymbol{\Pi}^{0,P}_{k-1}\nabla \boldsymbol{u}_h||^2_{L^2(P)}},$$

  the theoretical expected convergence rate is h^k (cf. (5.11));
- L^2*-pressure error*:

$$e^{p}_{L^2} := \sqrt{\sum_{P\in\Omega_h} ||p - p_h||^2_{L^2(P)}},$$

  the expected rate is h^k (cf. (5.12)).

6.3. *Numerical tests*

In this subsection, we consider three different tests. In the first two examples, we numerically verify the theoretical trend of all the errors for a Stokes and Navier–Stokes problem. Finally, we propose two benchmark examples for the Stokes equation with the property of having the velocity solution in the discrete space $\boldsymbol{V}_h$. It is well known that classical mixed FEMs lead in this situations to significant velocity errors, stemming from the velocity/pressure coupling in the error estimates. This effect is greatly reduced by the presented methods (cf. Theorem 5.1, estimate (5.11)).

Example 1. (Stokes Problem) In this paragraph, we solve the Stokes problem on the unit cube $[0\,,1]^3$, the discrete version being as in (5.9) but without the trilinear form $c_h(\cdot\,;\cdot,\cdot)$. We consider Neumann homogeneous boundary conditions on the faces associated with the planes $x = 0$ and $x = 1$. The load term and the Dirichlet boundary conditions on the remaining faces are chosen in such a way that the exact solution is

$$\boldsymbol{u}(x, y, z) := \begin{pmatrix} \sin(\pi x)\cos(\pi y)\cos(\pi z) \\ \cos(\pi x)\sin(\pi y)\cos(\pi z) \\ -2\cos(\pi x)\cos(\pi y)\sin(\pi z) \end{pmatrix}$$

and

$$p(x, y, z) := -\pi\cos(\pi x)\cos(\pi y)\cos(\pi z).$$

We consider the *Structured*, *CVT* and *Random* meshes. In Fig. 2, we show the behavior of the errors $e^{\boldsymbol{u}}_{H^1}$ and $e^{p}_{L^2}$. The slope of such errors are the expected ones, $O(h^k)$ see Theorem 5.1. Moreover, for each approximation degree k the convergence

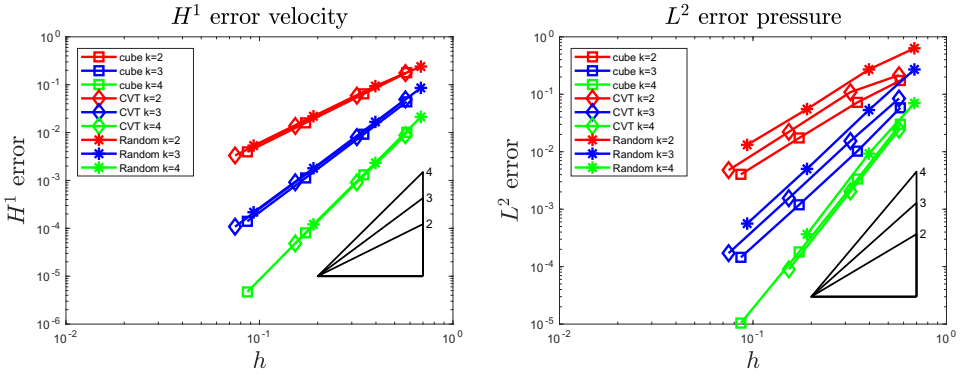

Fig. 2. Example 1 (Stokes problem): Convergence lines for *Structured*, *CVT* and *Random* meshes and degrees $k = 2, 3$ and 4.

lines associated with different meshes are close to each other and this represents a numerical evidence that the proposed method is robust with respect to the adopted meshes.

Example 2. (Navier–Stokes Problem) In this paragraph, we consider the Navier–Stokes problem described in Eq. (5.9) with Dirichlet boundary conditions. We consider the same discretization of the unit cube of the previous example, i.e. the set of meshes *Structured*, *CVT* and *Random*. We define the right-hand side and the boundary conditions in such a way that the exact solution is

$$\boldsymbol{u}(x,y,z) := \begin{pmatrix} \sin(\pi x)\cos(\pi y)\cos(\pi z) \\ \cos(\pi x)\sin(\pi y)\cos(\pi z) \\ -2\cos(\pi x)\cos(\pi y)\sin(\pi z) \end{pmatrix}$$

and

$$p(x,y,z) := \sin(2\pi x)\sin(2\pi y)\sin(2\pi z).$$

We solve the nonlinear problem by using standard Newton–Rapson iterations with a stopping criterion based on the displacement convergence test error with a tolerance `tol=1e-10`, i.e. until $||\mathbf{x}_n - \mathbf{x}_{n+1}|| < \texttt{tol}\,||\mathbf{x}_n||$ where $\mathbf{x}_n$ refers to the solution at the n-step. In Fig. 3, we show the convergence lines of the H^1 error on the velocity and the L^2 error on the pressure, respectively. In all these cases we have the predicted trend: h^k for the velocity and h^k for the pressure, see Theorem 5.1. Moreover, also in this case the lines are close to each other varying the mesh discretization, especially for the velocity solution. Note that, for the pressure solution and random meshes, higher order case $k = 3$, there seems to be a loss of accuracy at the second step. We believe this is due to difficulties related to the Newton convergence iterates (the associated linear system getting quite badly conditioned) since random meshes have a very bad geometry and we are reaching near the memory limit of our platform. We were unable to run a further step due to memory limits.

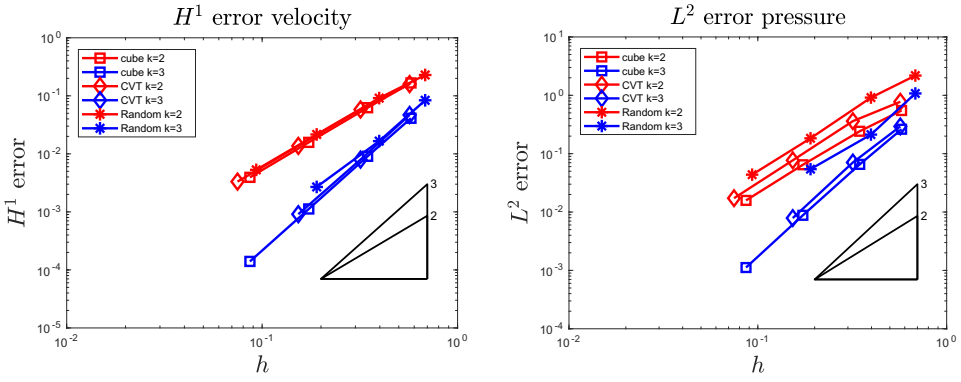

Fig. 3. Example 2 (Navier–Stokes problem): Convergence lines for *Structured*, *CVT* and *Random* meshes and degrees $k = 2$ and 3.

Improving this aspect, possibly by exploring more advanced solvers or changing the adopted virtual element basis,[34] is beyond the scope of this paper.

Example 3. (Benchmark Problems) In this paragraph, inspired by Ref. 47, we consider a particular example to numerically show an advantage of the proposed method. It is well known that the error on the velocity field of standard inf-sup stable elements for the Stokes equation is pressure-dependent.[23] Consequently, the accuracy of the discrete solution $\boldsymbol{u}_h$ is affected by the discrete pressure error. As already shown for the 2D case in Ref. 17, also in the 3D case we do not have such dependency on the error, i.e. the error on the discrete velocity field $\boldsymbol{u}_h$ does not depend on the pressure, but *only* on the velocity $\boldsymbol{u}$ and on the load term $\boldsymbol{f}$ (see Theorem 5.1, estimate (5.11)). Note that this method, although div-free, is not pressure-robust in the sense of Ref. 47 since the error on the velocities is indirectly affected by the pressure through the loading approximation term.[17] Nevertheless it is still much better than the inf-sup stable element in this respect, as the accuracy of the load approximation (being a known quantity) can be easily improved.

To numerically verify such property we consider two Stokes problems where the exact velocity field is contained in $\mathbf{V}_h$

$$\boldsymbol{u}(x,y,z) := \begin{pmatrix} kxz^{k-1} \\ kyz^{k-1} \\ (2-k)x^k + (2-k)y^k - 2z^k \end{pmatrix},$$

where k is the VEM approximation degree, but we vary the solution on the pressure. More specifically we will consider these two pressure solutions: a polynomial pressure

$$p_1(x,y,z) := x^k y + y^k z + z^k x - \frac{3}{2(k+1)},$$

H^1 error velocity

k	**Structured**	**Tetra**
2	1.0576e-13	7.2075e-13
3	2.7333e-13	1.1927e-12
4	1.5266e-12	2.2718e-10

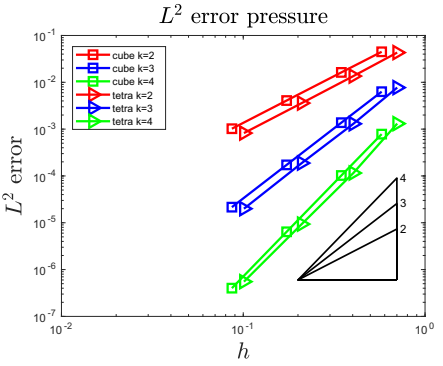

Fig. 4. Example 3 (Benchmark problem): The values of the errors $e^{\boldsymbol{u}}_{H^1}$ for the coarsest meshes of *Structured* and *Tetra* meshes, left, pressure convergence lines, right, for a Stokes problem where we consider p_1 as pressure.

and an analytic pressure

$$p_2(x, y, z) := \sin(2\pi x)\sin(2\pi y)\sin(2\pi z).$$

Note that in both cases, since $p_i \notin Q_h$ for $i = 1, 2$, a standard inf-sup stable element of analogous polynomial degree would obtain $O(h^k)$ error for the velocities in the H^1 norm even if $\boldsymbol{u} \in \mathbf{V}_h$. In the first case, the velocity is a polynomial vector field of degree k, while the pressure is a polynomial of degree k and the load term $\boldsymbol{f}$ is a polynomial of degree k. In such configuration the presented VEM scheme yields the exact solution up to machine precision for the velocity field. Indeed, the velocity virtual element space contains polynomials of degree k and, since the load term is a polynomial of degree k, the term $\mathcal{H}(\boldsymbol{f}, \nu)$ in Eq. (5.11) is close to the machine precision, i.e. we approximate exactly the load term $\boldsymbol{f}$ (cf. definition (5.7)), so the error on $\boldsymbol{u}$ is close to the machine precision.

In table of Fig. 4(left), we collect the errors $e^{\boldsymbol{u}}_{H^1}$ only for the coarsest meshes composed by 27 and 68 elements for the *Structured* and *Tetra* meshes, respectively.

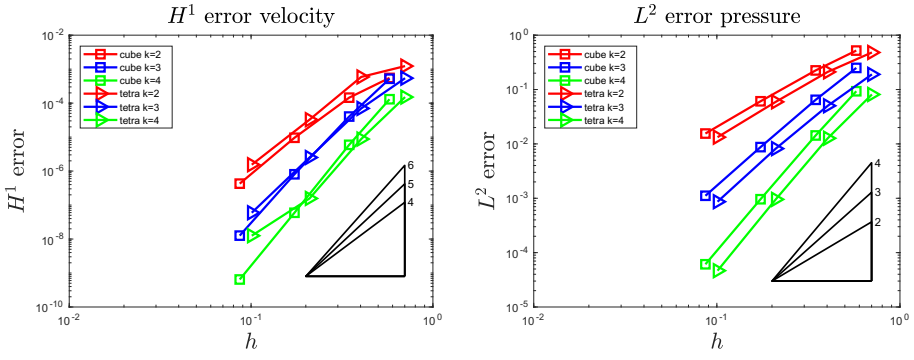

Fig. 5. Example 3 (Benchmark): Convergence lines for a Stokes problem with *Structured* and *Tetra* meshes where we consider a sinusoidal pressure function, p_2.

In the second case the velocity is still a polynomial of degree k, but, since the pressure is a sinusoidal function, now the right-hand side $\boldsymbol{f}$ is not a polynomial. Even if the velocity virtual element space contains the polynomials of degree k, i.e., the velocity error is affected by the polynomial approximation of the load term, therefore we expect is h^{k+2}, which is still much better than $O(h^k)$.

In Fig. 5, we show the convergence lines for both $e^{\boldsymbol{u}}_{H^1}$ and $e^{p}_{L^2}$. The error trends are the expected ones: we get $O(h^4)$, $O(h^5)$ and $O(h^6)$ for degrees $k = 2, 3$ and 4, respectively, while we get $O(h^k)$ for the pressure. In the last step of the H^1 norm error, the error is higher than expected (this behavior is due to machine algebra effects since we are in a range of very small errors).

Appendix A

The aim of this appendix is addressing the well-posedness of the biharmonic problem with the non-homogeneous boundary conditions stated in definition (3.17). Indeed, although in the literature one can find many references for the homogeneous case,[4,20,43] to the authors best knowledge the extension to the non-homogeneous case is labeled as feasible but never explicited. For completeness, we here provide the details.

We first recall that the space $\boldsymbol{\Psi}(P)$ is provided with the norm[43]:

$$\|\boldsymbol{\psi}\|^2_{\boldsymbol{\Psi}(P)} := \|\boldsymbol{\psi}\|^2_{0,P} + \|\mathbf{curl}\,\boldsymbol{\psi}\|^2_{1,P} + \|\mathrm{div}\,\boldsymbol{\psi}\|^2_{1,P}.$$

Moreover, if P is a contractible polyhedron the following bounds hold (Lemma 5.2 in Ref. 43)

$$\|\boldsymbol{\psi}\|^2_{0,P} + \|\boldsymbol{\Delta}\,\boldsymbol{\psi}\|^2_{0,P} \lesssim \|\boldsymbol{\psi}\|^2_{\boldsymbol{\Psi}(P)} \lesssim \|\boldsymbol{\Delta}\,\boldsymbol{\psi}\|^2_{0,P} \quad \text{for all } \boldsymbol{\psi} \in \boldsymbol{\Psi}_0(P). \tag{A.1}$$

We start our analysis by recalling the following result concerning the case of homogeneous boundary conditions (see Lemma 5.1 in Ref. 43).

Lemma A.1. *Let P be a contractible polyhedron and let $\boldsymbol{F}\colon \boldsymbol{\Psi}_0(P) \to \mathbb{R}$ be a given linear continuous functional. The biharmonic problem coupled with homogeneous boundary conditions*

$$\begin{cases} \text{find } \boldsymbol{\varphi} \in \boldsymbol{\Psi}_0(P), & \text{such that} \\ \displaystyle\int_P \boldsymbol{\Delta}\,\boldsymbol{\varphi} \cdot \boldsymbol{\Delta}\,\boldsymbol{\psi}\,\mathrm{d}P = \boldsymbol{F}(\boldsymbol{\psi}) & \text{for all } \boldsymbol{\psi} \in \boldsymbol{\Psi}_0(P), \end{cases}$$

has a unique solution $\boldsymbol{\varphi}$.

The next theorem extends the well-posedness result of the previous lemma to the case of inhomogeneous boundary conditions.

Theorem A.1. *Let P be a contractible polyhedron and let*

- $\boldsymbol{h} \in [L^2(\partial P)]^3$ *such that for any f, f_1, $f_2 \in \partial P$ and for any $e \subseteq f_1 \cap f_2$*

$$\boldsymbol{h}_\tau \in H(\mathrm{div}_f, f) \cap H(\mathrm{rot}_f, f) \quad \textit{and} \quad (\boldsymbol{h}_{f_1} \cdot \boldsymbol{t}_e)_{|e} = (\boldsymbol{h}_{f_2} \cdot \boldsymbol{t}_e)_{|e},$$

- $\boldsymbol{g} \in [H^{1/2}(\partial P)]^3$ *such that*

$$\boldsymbol{g} \cdot \boldsymbol{n}_P^f = \mathrm{rot}_f \boldsymbol{h}_\tau \quad \textit{for any } f \in \partial P, \tag{A.2}$$

- $\boldsymbol{f} \in [L^2(P)]^3 \cap \boldsymbol{Z}(P)$.

The following biharmonic problem has a unique solution $\boldsymbol{\varphi}$

$$\begin{cases} \textit{find } \boldsymbol{\varphi} \in \boldsymbol{\Psi}(P), & \textit{such that} \\ \displaystyle\int_P \boldsymbol{\Delta}\,\boldsymbol{\varphi} \cdot \boldsymbol{\Delta}\,\boldsymbol{\psi}\,\mathrm{d}P = \int_P \boldsymbol{f} \cdot \boldsymbol{\psi}\,\mathrm{d}P & \textit{for all } \boldsymbol{\psi} \in \boldsymbol{\Psi}_0(P), \\ \displaystyle\int_{\partial P} \boldsymbol{\varphi} \cdot \boldsymbol{n}_P\,\mathrm{d}f = 0, & \\ \boldsymbol{\varphi}_\tau = \boldsymbol{h}_\tau & \textit{on } \partial P, \\ \mathbf{curl}\,\boldsymbol{\varphi} = \boldsymbol{g} & \textit{on } \partial P. \end{cases} \tag{A.3}$$

Proof. Let us consider the following auxiliary problem

$$\begin{cases} \text{find } \boldsymbol{\varphi}^\partial \in \boldsymbol{\Psi}(P), & \text{such that} \\ \displaystyle\int_{\partial P} \boldsymbol{\varphi}^\partial \cdot \boldsymbol{n}_P\,\mathrm{d}f = 0, & \\ \boldsymbol{\varphi}_\tau^\partial = \boldsymbol{h}_\tau & \text{on } \partial P, \\ \mathbf{curl}\,\boldsymbol{\varphi}^\partial = \boldsymbol{g} & \text{on } \partial P. \end{cases} \tag{A.4}$$

We construct by hand a suitable $\boldsymbol{\varphi}^\partial$ that satisfies (A.4).

Let us consider the Stokes-type problem defined on P

$$\begin{cases} \text{find } (\boldsymbol{u}, p) \in [H^1(P)]^3 \times L_0^2(P), & \text{such that} \\ -\boldsymbol{\Delta}\,\boldsymbol{u} + \nabla p = \boldsymbol{0} & \text{in } P, \\ \mathrm{div}\,\boldsymbol{u} = 0 & \text{in } P, \\ \boldsymbol{u} = \boldsymbol{g} & \text{on } \partial P \end{cases} \tag{A.5}$$

then by Theorem 3.4 in Ref. 43, there exists a vector potential $\boldsymbol{\varphi}^{\boldsymbol{g}}$ (possibly not unique) satisfying

$$\begin{cases} \boldsymbol{\varphi}^{\boldsymbol{g}} \in \boldsymbol{\Psi}(P), & \text{such that} \\ \mathbf{curl}\,\boldsymbol{\varphi}^{\boldsymbol{g}} = \boldsymbol{u} & \text{in } P, \\ \mathrm{div}\,\boldsymbol{\varphi}^{\boldsymbol{g}} = 0 & \text{in } P. \end{cases} \tag{A.6}$$

Moreover, (A.6) implies that $-\boldsymbol{\Delta}\,\boldsymbol{\varphi}^{\boldsymbol{g}} = \mathbf{curl}\,\boldsymbol{u}$, thus the following stability estimate holds[23]:

$$\|\boldsymbol{\Delta}\,\boldsymbol{\varphi}^{\boldsymbol{g}}\|_{0,P} = \|\mathbf{curl}\,\boldsymbol{u}\|_{0,P} \leq \|\boldsymbol{u}\|_{1,P} \lesssim |\boldsymbol{g}|_{1/2,\partial P}. \tag{A.7}$$

Notice that from (A.2), (2.4), (A.6) and (A.5), on each face $f \in \partial P$, we infer

$$\mathrm{rot}_f(\boldsymbol{h} - \boldsymbol{\varphi}^{\boldsymbol{g}})_\tau = \mathrm{rot}_f\, \boldsymbol{h}_\tau - \mathrm{rot}_f\, \boldsymbol{\varphi}^{\boldsymbol{g}}_\tau = \boldsymbol{g} \cdot \boldsymbol{n}^f_P - (\mathbf{curl}\, \boldsymbol{\varphi}^{\boldsymbol{g}})_{|f} \cdot \boldsymbol{n}^f_P = 0.$$

Therefore, it can be shown that there exists $\zeta \in H^1(\partial P)$ such that

$$\nabla_f \zeta_\tau = (\boldsymbol{h} - \boldsymbol{\varphi}^{\boldsymbol{g}})_\tau \quad \text{on any } f \in \partial P. \tag{A.8}$$

Now we consider the elliptic problem

$$\begin{cases} \Delta\omega = 0 & \text{in } P, \\ \omega = \zeta & \text{on } \partial P. \end{cases}$$

We observe that $\boldsymbol{\varphi}^{\boldsymbol{h}} := \nabla\, \omega$ satisfies, also recalling (A.8),

$$\begin{cases} \boldsymbol{\varphi}^{\boldsymbol{h}} \in \boldsymbol{\Psi}(P), & \text{such that} \\ \mathbf{curl}\, \boldsymbol{\varphi}^{\boldsymbol{h}} = \mathbf{0} & \text{in } P, \\ \mathrm{div}\, \boldsymbol{\varphi}^{\boldsymbol{h}} = 0 & \text{in } P, \\ \boldsymbol{\varphi}^{\boldsymbol{h}}_\tau = \boldsymbol{h} - \boldsymbol{\varphi}^{\boldsymbol{g}}_\tau & \text{on } \partial P. \end{cases} \tag{A.9}$$

From (A.9) it holds that

$$\boldsymbol{\Delta}\, \boldsymbol{\varphi}^{\boldsymbol{h}} = \mathbf{0}. \tag{A.10}$$

By construction $\boldsymbol{\varphi}^{\partial} := \boldsymbol{\varphi}^{\boldsymbol{g}} + \boldsymbol{\varphi}^{\boldsymbol{h}}$ satisfies (A.4) and from (A.7) and (A.10) it holds that

$$\|\boldsymbol{\Delta}\, \boldsymbol{\varphi}^{\partial}\|_{0,P} \lesssim |\boldsymbol{g}|_{1/2,\partial P}. \tag{A.11}$$

We consider now the homogeneous auxiliary problem

$$\begin{cases} \text{find } \boldsymbol{\varphi}^{\mathrm{hom}} \in \boldsymbol{\Psi}_0(P), & \text{such that} \\ \displaystyle\int_P \boldsymbol{\Delta}\, \boldsymbol{\varphi}^{\mathrm{hom}} \cdot \boldsymbol{\Delta}\, \boldsymbol{\psi}\, \mathrm{d}P = \int_P \boldsymbol{f} \cdot \boldsymbol{\psi}\, \mathrm{d}P - \int_P \boldsymbol{\Delta}\, \boldsymbol{\varphi}^{\partial} \cdot \boldsymbol{\Delta}\, \boldsymbol{\psi}\, \mathrm{d}P & \text{for all } \boldsymbol{\psi} \in \boldsymbol{\Psi}_0(P). \end{cases} \tag{A.12}$$

Being $\boldsymbol{f} \in [L^2(P)]^3$, from (A.11), (A.1) and Lemma A.1, problem (A.12) has a unique solution $\boldsymbol{\varphi}^{\mathrm{hom}} \in \boldsymbol{\Psi}_0(P)$. It is straightforward to see that $\boldsymbol{\varphi} := \boldsymbol{\varphi}^{\mathrm{hom}} + \boldsymbol{\varphi}^{\partial}$ is a solution to problem (A.3). The uniqueness easily follows from the norm equivalence (A.1). □

Acknowledgments

The authors were partially supported by the European Research Council through the H2020 Consolidator Grant (Grant No. 681162) CAVE, Challenges and Advancements in Virtual Elements. This support is gratefully acknowledged.

References

1. R. A. Adams, *Sobolev Spaces*, Pure and Applied Mathematics, Vol. 65 (Academic Press, 1975).
2. B. Ahmad, A. Alsaedi, F. Brezzi, L. D. Marini and A. Russo, Equivalent projectors for virtual element methods, *Comput. Math. Appl.* **66** (2013) 376–391.
3. F. Aldakheel, B. Hudobivnik, A. Hussein and P. Wriggers, Phase-field modeling of brittle fracture using an efficient virtual element scheme, *Comput. Methods Appl. Mech. Eng.* **341** (2018) 443–466.
4. C. Amrouche, C. Bernardi, M. Dauge and V. Girault, Vector potentials in three-dimensional non-smooth domains, *Math. Methods Appl. Sci.* **21** (1998) 823–864.
5. P. F. Antonietti, L. Beirão da Veiga, D. Mora and M. Verani, A stream virtual element formulation of the stokes problem on polygonal meshes, *SIAM J. Numer. Anal.* **52** (2014) 386–404.
6. P. F. Antonietti, G. Manzini and M. Verani, The fully nonconforming virtual element method for biharmonic problems, *Math. Models Methods Appl. Sci.* **28** (2018) 387–407.
7. D. N. Arnold, R. S. Falk and R. Winther, Differential complexes and stability of finite element methods. I. The de Rham complex, in *Compatible Spatial Discretizations, IMA Volumes in Mathematics and its Applications*, Vol. 142 (Springer, 2006), pp. 24–46.
8. D. N. Arnold, R. S. Falk and R. Winther, Finite element exterior calculus, homological techniques, and applications, *Acta Numer.* **15** (2006) 1–155.
9. D. N. Arnold, R. S. Falk and R. Winther, Finite element exterior calculus: From Hodge theory to numerical stability, *Bull. Amer. Math. Soc.* (*N.S.*) **47** (2010) 281–354.
10. L. Beirão da Veiga, F. Brezzi, A. Cangiani, G. Manzini, L. D. Marini and A. Russo, Basic principles of virtual element methods, *Math. Models Methods Appl. Sci.* **23** (2013) 199–214.
11. L. Beirão da Veiga, F. Brezzi, F. Dassi, L. D. Marini and A. Russo, A family of three-dimensional virtual elements with applications to magnetostatics, *SIAM J. Numer. Anal.* **56** (2018) 2940–2962.
12. L. Beirão da Veiga, F. Brezzi, L. D. Marini and A. Russo, The Hitchhiker's guide to the virtual element method, *Math. Models Methods Appl. Sci.* **24** (2014) 1541–1573.
13. L. Beirão da Veiga, F. Brezzi, L. D. Marini and A. Russo, $H(\mathrm{div})$ and $H(\mathbf{curl})$-conforming virtual element methods, *Numer. Math.* **133** (2016) 303–332.
14. L. Beirão da Veiga, F. Brezzi, L. D. Marini and A. Russo, Serendipity nodal VEM spaces, *Comput. Fluids* **141** (2016) 2–12.
15. L. Beirão da Veiga, F. Dassi and A. Russo, High-order virtual element method on polyhedral meshes, *Comput. Math. Appl.* **74** (2017) 1110–1122.
16. L. Beirão da Veiga, C. Lovadina and A. Russo, Stability analysis for the virtual element method, *Math. Models Methods Appl. Sci.* **27** (2017) 2557–2594.
17. L. Beirão da Veiga, C. Lovadina and G. Vacca, Divergence free virtual elements for the stokes problem on polygonal meshes, *ESAIM Math. Model. Numer. Anal.* **51** (2017) 509–535.
18. L. Beirão da Veiga, C. Lovadina and G. Vacca, Virtual elements for the Navier–Stokes problem on polygonal meshes, *SIAM J. Numer. Anal.* **56** (2018) 1210–1242.
19. L. Beirão da Veiga, D. Mora and G. Vacca, The stokes complex for virtual elements with application to Navier–Stokes flows, *J. Sci. Comput.* **81** (2019) 990–1018.
20. A. Bendali, J. M. Domínguez and S. Gallic, A variational approach for the vector potential formulation of the stokes and Navier–Stokes problems in three-dimensional domains, *J. Math. Anal. Appl.* **107** (1985) 537–560.

21. S. Berrone and A. Borio, A residual *a posteriori* error estimate for the virtual element method, *Math. Models Methods Appl. Sci.* **27** (2017) 1423–1458.
22. S. Bertoluzza, M. Pennacchio and D. Prada, BDDC and FETI-DP for the virtual element method, *Calcolo* **54** (2017) 1565–1593.
23. D. Boffi, F. Brezzi and M. Fortin, *Mixed Finite Element Methods and Applications*, Springer Series in Computational Mathematics, Vol. 44 (Springer, 2013).
24. L. Botti, D. A. Di Pietro and J. Droniou, A hybrid high-order discretisation of the Brinkman problem robust in the Darcy and Stokes limits, *Comput. Methods Appl. Mech. Eng.* **341** (2018) 278–310.
25. S. C. Brenner, Q. Guan and L. Y. Sung, Some estimates for virtual element methods, *Comput. Methods Appl. Math.* **17** (2017) 553–574.
26. S. C. Brenner and L. Y. Sung, Virtual element methods on meshes with small edges or faces, *Math. Models Methods Appl. Sci.* **28** (2018) 1291–1336.
27. A. Buffa, J. Rivas, G. Sangalli and R. Vázquez, Isogeometric discrete differential forms in three dimensions, *SIAM J. Numer. Anal.* **49** (2011) 818–844.
28. E. Cáceres, G. N. Gatica and F. A. Sequeira, A mixed virtual element method for quasi-Newtonian stokes flows, *SIAM J. Numer. Anal.* **56** (2018) 317–343.
29. A. Cangiani, V. Gyrya and G. Manzini, The nonconforming virtual element method for the stokes equations, *SIAM J. Numer. Anal.* **54** (2016) 3411–3435.
30. S. Cao and L. Chen, Anisotropic error estimates of the linear virtual element method on polygonal meshes, *SIAM J. Numer. Anal.* **56** (2018) 2913–2939.
31. L. Chen and F. Wang, A divergence free weak virtual element method for the stokes problem on polytopal meshes, *J. Sci. Comput.* **78** (2019) 864–886.
32. S. H. Christiansen and K. Hu, Generalized finite element systems for smooth differential forms and stokes problem, *Numer. Math.* **140** (2018) 327–371.
33. B. Cockburn, G. Fu and W. Qiu, A note on the devising of superconvergent HDG methods for stokes flow by M-decompositions, *IMA J. Numer. Anal.* **37** (2017) 730–749.
34. F. Dassi and L. Mascotto, Exploring high-order three dimensional virtual elements: Bases and stabilizations, *Comput. Math. Appl.* **75** (2018) 3379–3401.
35. F. Dassi and G. Vacca, Bricks for mixed high-order virtual element method: Projectors and differential operators, *Appl. Numer. Math.* (2019), doi.org/10.1016/j.apnum.2019.03.014.
36. L. Demkowicz and A. Buffa, H^1, $H(\mathrm{curl})$ and $H(\mathrm{div})$-conforming projection-based interpolation in three dimensions. Quasi-optimal p-interpolation estimates, *Comput. Methods Appl. Mech. Eng.* **194** (2005) 267–296.
37. L. Demkowicz, P. Monk, L. Vardapetyan and W. Rachowicz, de Rham diagram for *hp* finite element spaces, *Comput. Math. Appl.* **39** (2000) 29–38.
38. D. A. Di Pietro and S. Krell, A hybrid high-order method for the steady incompressible Navier–Stokes problem, *J. Sci. Comput.* **74** (2018) 1677–1705.
39. J. A. Evans and T. J. R. Hughes, Isogeometric divergence-conforming B-splines for the steady Navier–Stokes equations, *Math. Models Methods Appl. Sci.* **23** (2013) 1421–1478.
40. R. S. Falk and M. Neilan, Stokes complexes and the construction of stable finite elements with pointwise mass conservation, *SIAM J. Numer. Anal.* **51** (2013) 1308–1326.
41. A. L. Gain, G. H. Paulino, L. S. Duarte and I. F. M. Menezes, Topology optimization using polytopes, *Comput. Methods Appl. Mech. Eng.* **293** (2015) 411–430.
42. G. N. Gatica, M. Munar and F. A. Sequeira, A mixed virtual element method for a nonlinear Brinkman model of porous media flow, *Calcolo* **55** (2018) Art. 21, 36.

43. V. Girault and P.-A. Raviart, *Finite Element Approximation of the Navier–Stokes Equations*, Lecture Notes in Mathematics, Vol. 749 (Springer-Verlag, 1979).
44. J. Guzmán and M. Neilan, Conforming and divergence-free stokes elements on general triangular meshes, *Math. Comp.* **83** (2014) 15–36.
45. J. Guzmán and M. Neilan, Inf-Sup stable finite elements on barycentric refinements producing divergence–free approximations in arbitrary dimensions, *SIAM J. Numer. Anal.* **56** (2018) 2826–2844.
46. V. John, A. Linke, C. Merdon, M. Neilan and L. G. Rebholz, On the divergence constraint in mixed finite element methods for incompressible flows, *SIAM Rev.* **59** (2017) 492–544.
47. A. Linke and C. Merdon, On velocity errors due to irrotational forces in the Navier–Stokes momentum balance, *J. Comput. Phys.* **313** (2016) 654–661.
48. A. Linke and C. Merdon, Pressure-robustness and discrete Helmholtz projectors in mixed finite element methods for the incompressible Navier–Stokes equations, *Comput. Methods Appl. Mech. Eng.* **311** (2016) 304–326.
49. K. Lipnikov, D. Vassilev and I. Yotov, Discontinuous Galerkin and mimetic finite difference methods for coupled Stokes–Darcy flows on polygonal and polyhedral grids, *Numer. Math.* **126** (2014) 321–360.
50. X. Liu, J. Li and Z. Chen, A nonconforming virtual element method for the stokes problem on general meshes, *Comput. Methods Appl. Mech. Eng.* **320** (2017) 694–711.
51. L. Mascotto, I. Perugia and A. Pichler, Non-conforming harmonic virtual element method: h- and p-versions, *J. Sci. Comput.* **77** (2018) 1874–1908.
52. M. Neilan, Discrete and conforming smooth de Rham complexes in three dimensions, *Math. Comp.* **84** (2015) 2059–2081.
53. M. Neilan and D. Sap, Stokes elements on cubic meshes yielding divergence-free approximations, *Calcolo* **53** (2016) 263–283.
54. A. Quarteroni and A. Valli, *Numerical Approximation of Partial Differential Equations*, Springer Series in Computational Mathematics, Vol. 23 (Springer-Verlag, 1994).
55. C. H. Rycroft, Voro++: A three-dimensional voronoi cell library in c++, *Chaos* **19** (2009) 041111.
56. H. Si, Tetgen, A delaunay-based quality tetrahedral mesh generator, *ACM Trans. Math. Softw.* (*TOMS*) **41** (2015) 11.
57. G. Vacca, An H^1-conforming virtual element for Darcy and Brinkman equations, *Math. Models Methods Appl. Sci.* **28** (2018) 159–194.